Framework for the Buckling Optimization of Variable-Angle Tow Composite Plates

Zhangming Wu,* Gangadharan Raju,† and Paul M. Weaver‡
University of Bristol, Bristol, England BS8 1TR, United Kingdom

DOI: 10.2514/1.J054029

Variable-angle tow describes fibers in a composite lamina that have been steered curvilinearly. In doing so, substantially enlarged freedom for stiffness tailoring of composite laminates is enabled. Variable-angle tow composite structures have been shown to have improved buckling and postbuckling load-carrying capability when compared to straight fiber composites. However, their structural analysis and optimal design is more computationally expensive due to the exponential increase in number of variables associated with spatially varying planar fiber orientations in addition to stacking sequence considerations. In this work, an efficient two-level optimization framework using lamination parameters as design variables has been enhanced and generalized to the design of variable-angle tow plates. New explicit stiffness matrices are found in terms of component material invariants and lamination parameters. The convex hull property of B-splines is exploited to ensure pointwise feasibility of lamination parameters. In addition, a set of new explicit closed-form expressions defines the feasible region of two in-plane and two out-of-plane lamination parameters, which are used for the design of orthotropic laminates. Finally, numerical examples of plates under compression loading with different boundary conditions and aspect ratios are investigated. Reliable optimal solutions demonstrate the robustness and computational efficiency of the proposed optimization methodology.

Nomenclature

A	=	matrix of in-plane stiffness (A_{ij})
a, b, h	=	length, width, and thickness of plate
$B_{rs}^{(x)}$, $B_{rs}^{(y)}$	=	x and y coordinates of control points for a B-spline
c_j	=	undetermined weight for a component of in-plane force loading
D	=	matrix of bending stiffness (D_{ij})
E_{iso}, ν_{iso}, D_{iso}	=	equivalent Young's modulus, Poisson's ratio, and bending stiffness of quasi-isotropic laminate
e	=	test variable in the trial function g
$\boldsymbol{F}$	=	vector of applied in-plane loading
f, g	=	trial functions for Schwarz inequality
$\bar{f}_i$	=	objective function or constraint function
H^L, H^U	=	lower and upper bounds of each hyperplane constraint
$\boldsymbol{h}$	=	$\{h_1, h_2, h_3, h_4, h_5\}$; vector for a hyperplane along the boundary of the feasible regions
K_{cr}^*	=	normalized buckling load of variable-angle tow plate
K_0^b, K_1^b, K_2^b	=	separate parts of bending stiffness matrix
K_{10}^s, K_{11}^s, $\cdots$	=	separate parts of stability stiffness matrix
K^b, K^s	=	bending stiffness matrix and stability matrix in buckling model
K^m	=	in-plane stiffness matrix in prebuckling model
k, Ξ	=	order (degree) and knot vector of B-splines
$\boldsymbol{N}$, $\boldsymbol{M}$	=	in-plane stress and bending moment resultants
$N_s^{(k)}$, $N_s^{(k)}$	=	B-spline basis functions
$(N_x^{\text{cr}})_{\text{iso}}$	=	critical buckling load of quasi-isotropic laminate
$(N_x^{\text{cr}})_{\text{vat}}$	=	critical buckling load of variable-angle tow laminate
R	=	plate aspect ratio (a/b)
s, t	=	directional variables for a general parabola
T_{mn}	=	fiber angle of variable-angle tow plate at a control point (P_{mn})
$\boldsymbol{U}$	=	vector of unknown coefficients for in-plane displacements
U_{pq}, V_{pq}, W_{pq}	=	undetermined coefficients for displacement fields
U_1, U_2, U_3, U_4, U_5	=	material invariants
$\boldsymbol{u}_0$	=	prescribed in-plane displacement loading
u^0, v^0	=	in-plane displacement at reference plane in x and y directions
$\bar{u}$, $\bar{v}$	=	B-spline parametric coordinates
w	=	out-of-plane deflection
w_i^A, w_i^D	=	weighting functions
$X^u(x)$, $Y^u(y)$	=	shape functions for in-plane displacement u^0
$X^v(x)$, $Y^v(y)$	=	shape functions for in-plane displacement v^0
$X^w(x)$, $Y^w(y)$	=	shape functions for out-of-plane displacement w
z, $\bar{z}$	=	direction along the thickness of a laminate
z_x, z_y	=	distance of a ply to the midplane
$\alpha^{(\mu)}$, $\beta^{(\mu)}$	=	upper and lower moving asymptotes
$\boldsymbol{\Gamma}$, $\Gamma_{rs}^{(\tau)}$	=	lamination parameters at a control point (P_{rs})
Δ_x	=	end-shortening displacement along x direction
ϵ^0, κ	=	midplane strains and out-of-plane curvatures

Received 25 November 2014; revision received 5 May 2015; accepted for publication 26 May 2015; published online 30 July 2015.

*Postdoctoral Researcher, Advanced Composite Centre for Innovation and Science, Department of Aerospace Engineering, Queen's Building, University Walk.

†Research Assistant, Advanced Composite Centre for Innovation and Science, Department of Aerospace Engineering, Queen's Building, University Walk.

‡Professor in Lightweight Structures, Advanced Composite Centre for Innovation and Science, Department of Aerospace Engineering, Queen's Building, University Walk. Member AIAA.

$\theta(x, y)$ = variation of fiber angle of a variable-angle tow layer
λ (λ_{cr}) = eigenvalue of buckling model
μ, ν = indices of the outer and inner iterations in a globally convergent method of moving asymptotes routine
ξ_1^A, ξ_2^A = in-plane lamination parameters
ξ_1^D, ξ_2^D = out-of-plane lamination parameters
τ = $1(\xi_1^A)$, $2(\xi_2^A)$, $3(\xi_1^D)$, and $4(\xi_2^D)$
$\Psi(\boldsymbol{x}, \boldsymbol{y})$ = general shape function

I. Introduction

ADVANCED tow placement techniques allow the fiber (tow) to be placed curvilinearly within a lamina and, in doing so, enable the designer to take advantage of the directional properties of composite laminates. The concept of tow steering can be applied to the design of lightweight structures with potentially enhanced performance for aerospace applications [1–4]. In the preliminary design of long and slender aerospace structures, buckling resistance is often considered as a primary design criterion. It has been reported previously that the buckling load-carrying capacity of variable-angle tow (VAT) plates can be substantially improved when the in-plane prebuckling stresses that result from the variable stiffness are redistributed beneficially [2,3,5]. In contrast to the benefits offered by VAT, the optimal design of VAT laminates is a difficult task to undertake due to the increased design choice available to the designer for pointwise stiffness tailoring. The design of VAT laminates involves a large number of variables, as one has to determine the layup sequence at each point in the structure. The aim of this work is to develop a rapid, yet efficient, optimization framework to design VAT composite plates for maximum buckling load.

Ghiasi et al. [6] presented a thorough review of different optimization techniques for the design of variable stiffness composite plates, in which it was concluded that the multilevel optimization method is recommended due to its highly computational efficiency. Setoodeh et al. [7] used a reciprocal approximation method to design VAT plates for maximum buckling load and used finite element nodal fiber angles as design variables. Wu et al. [3] proposed a general control-point design scheme to describe a continuous variation of fiber angles, where the VAT configuration was optimized for maximum buckling load. However, the objective function in terms of fiber angle or fiber trajectory was highly nonconvex and the optimization process was likely to get trapped in local optima. To overcome these problems, the approach of using lamination parameters as design variables was shown to be an effective way to solve the optimization problem of variable stiffness laminates [5,8]. Lamination parameters [9] are evaluated by integrating the trigonometric functions of the ply orientation across the thickness of the plate. Usage of lamination parameters to represent composite layups not only results in a reduction of design variables but also offers possibly the largest convex design space. In addition, an optimization process can focus on the design of stiffness properties irrespective of laminate configuration (stacking sequence and fiber orientations). The advantage of using lamination parameters over using ply angles as design variables to perform the optimal design of constant-stiffness composite laminates has been reported in previous works [10–12]. The primary benefit arises from representing laminate stiffness as linear combinations of both material invariants and lamination parameters, which can lead to convex design spaces that enable efficient gradient-based optimizers to find global optima. Lamination parameters have also been successfully applied to the design of variable stiffness composite structures. Setoodeh et al. [13] and Abdalla et al. [14] optimized the in-plane stiffness and natural frequency of variable stiffness plates using lamination parameters, respectively. Ijsselmuiden et al. [5,15] presented a sophisticated framework based on finite element modeling and a successive approximation optimization technique [16] to perform the design of variable stiffness structures for maximum buckling load. All of these works [5,14,17] rely on a finite element design scheme, in which the local lamination parameters (design variables) are piecewise constant and associated with each element/node. However, the element-based optimization method may suffer from the increasing number of design variables and nonsmooth distribution of the lamination parameters unless an additional smoothing constraint is applied.

Furthermore, the values of 12 lamination parameters are not completely independent and are linked by a particular layup. Constraints that define the design space (feasible region) of lamination parameters are needed for an optimization process. Currently, the closed-form expressions that can exactly define the complete feasible region of 12 lamination parameters remain unknown. Miki and Sugiyama [10] first derived the parabolic relation of two in-plane or two out-of-plane lamination parameters. Later, Fukunaga and Sekine [18] further obtained closed-form expressions that could represent the feasible regions of the four in-plane and four out-of-plane lamination parameters. The pioneering work of Grenestedt and Gudmundson [19] proved the convexity of the feasible region of lamination parameters (also for the case of variable stiffness) and proposed a variational approach to evaluate the feasible region numerically. In the design of VAT laminates, the value of each lamination parameter varies continuously across the planform and the corresponding feasibility constraints should be satisfied at every point. Hence, an accurate bound for the feasible region of lamination parameters is necessary in the design of VAT laminates. Setoodeh et al. [20] proposed a convex hull approach to numerically represent the feasible region in terms of a large number (37,126) of linear algebraic equations (hyperplanes). Based on Bloomfield et al.'s work [21], we derive a small number of new explicit nonlinear expressions that give a relatively accurate boundary for the feasible region of these four lamination parameters, which is sufficient to define orthotropic VAT laminates.

The main objective of this paper is to introduce an optimization framework that employs B-splines to define the spatial variation of lamination parameters (variable stiffness). B-spline or nonuniform rational B-spline (NURBS) techniques that have been widely used in CAD systems [22] are able to represent complex geometries (variations) using relatively few design variables. A given degree B-spline curve/surface is determined by a set of control points and a prescribed knot vector. The control points are distributed over the plate domain, and the design variables (lamination parameters) are associated with each control point. The design flexibility is adjusted by altering the number and position of control points, the degree, and the knot vector of spline functions. This approach of defining the spatial variation of A, D stiffness matrices using B-spline functions is inspired by isogeometric analysis [23,24]. However, we do not need the complexity of NURBS functions and limit our choice to B-splines to represent lamination parameter variation because we only exploit the smoothness and convex properties. Compared with the discretized finite element approach, using B-splines to represent the spatial variation of lamination parameters requires less design variables and leads to a continuous and smooth distribution. In addition, the convex hull property of B-splines enforces the spatially varying lamination parameter across the planform of the plate to be fully constrained inside the feasible region, provided that the lamination parameters at the control points satisfy all the nonlinear constraints. Using B-splines avoids the problem of satisfying a large number of feasibility constraints at an infinite number of points in the plate that results in a cumbersome semi-infinite programming problem. In recent work, isogeometric techniques [25] have been applied to model and design VAT laminates with B-spline (or NURBS) format stiffness variation using finite element analysis as the structural tool. Our approach uses a more computationally efficient structural model than shown in [3], but it is not as versatile for complex geometries. In addition, we decouple the discretization scheme for the design of VAT layers from the structural modeling of VAT plates. However, the finite element approach including the isogeometric technique adopts the same discretization scheme for both the design and the structural model. Such an approach is efficient only where the optimal mesh size for structural analysis is the same as that needed for design and optimization. In our experience, we do not require as refined a mesh for optimization as is needed for analysis,

allowing us to use control-point variables used in optimization to be more sparsely distributed than that in the structural mesh.

For buckling or vibration optimization problems, the objective function expressed in terms of lamination parameters is much less ill conditioned (and can often be convex [19]) than using layer angles as the design variables. The revised objective function together with the convex design space reduces the complexity and computational time/efforts effectively. In this work, a gradient-based algorithm called the globally convergent method of moving asymptotes (GCMMA) [26] is adopted. The GCMMA employs a successive convex approximation technique, in which the objective functions and nonlinear constraints are replaced by a sequence of conservative convex separable approximations (subproblem) based on gradient information, and these subproblems are created and solved iteratively until a desired convergence is achieved. The approximation concept, introduced by Schmit and Farshi [27] and Schmit and Miura [28], has been extensively studied [29] and is a well-established technique for structural optimization. In previous works, the first-order Taylor series expansion [30], a reciprocal approximation [31], or a mixed-variable linearization were successively introduced to approximate the nonlinear objective/constraint functions at a local design point. The mixed-variable approach is more conservative than the former two methods, and it is a convex problem that can be readily solved by dual methods [32]. Later, Svanberg [33] developed a new method, named the method of moving asymptotes (MMA), for the convex and conservative approximation that could stabilize the optimization process through using two artificial asymptotes. The MMA was further developed for yielding a global convergent solution and is named GCMMA. In a GCMMA, additional damping factors are introduced to ensure a strict convexity of subproblems and the conservativeness is further checked iteratively.

In the current work, the buckling optimization of VAT plates is carried out within an enhanced two-level strategy, which advances the optimization framework first proposed by Yamazaki [34] and further developed by Diaconu and Weaver [35], Herencia et al. [36], and Bloomfield et al. [37] for straight fiber composites. At the first step, structural analysis is conducted using a Rayleigh–Ritz method in which novel explicit expressions for plate-level stiffness matrices were written in terms of component material invariants and lamination parameters. The spatially varying laminate stiffness, and therefore lamination parameter, distribution of VAT plates was represented using B-splines. Subsequently, a gradient-based method (GCMMA) was used to determine the optimal lamination parameters at each control point for the maximum buckling load. The convergence of the optimization process was studied by gradually increasing the number of the control points. Note, that the convexity of B-splines between control points guarantees feasibility of VAT layups if feasibility constraints on the lamination parameters have been satisfied at the control points. It is for this reason we choose B-splines to represent lamination parameter variation across the domain. At the end of the first step, we recover a smooth, continuous variation of lamination parameters that satisfies feasibility constraints on their values. At the second step, smooth, spatially varying distributions of fiber-orientation angles are retrieved from the target lamination parameters using a genetic algorithm (GA) in a similar way to that done previously [34,35]. The two-level approach provides an efficient way to solve the optimization problem, especially for VAT laminates. Furthermore, the lamination parameters guided design process allows the best possible laminate configuration to be determined, both theoretically (first-level) and that can be realized (second-level). The proposed optimization framework for the design of VAT laminates is used subsequently to determine the optimal fiber angle distribution for maximizing the buckling performance under different boundary conditions and loading cases.

II. Lamination Parameters

A. Definition of Lamination Parameters

Considering classical lamination theory, the constitutive equation of a VAT plate is given by

$$\begin{pmatrix} \boldsymbol{N} \\ \boldsymbol{M} \end{pmatrix} = \begin{bmatrix} A(\boldsymbol{x},\boldsymbol{y}) & B(x,y) \\ B^T(x,y) & D(\boldsymbol{x},\boldsymbol{y}) \end{bmatrix} \begin{pmatrix} \epsilon^0 \\ \kappa \end{pmatrix} \tag{1}$$

The in-plane, coupling, and bending stiffness matrices are functions of x and y for VAT plates, denoted by $A(\boldsymbol{x},\boldsymbol{y})$, $B(x,y)$, and $D(\boldsymbol{x},\boldsymbol{y})$, respectively. The stiffness matrices are expressed as a linear combination of lamination parameters and material invariants. In the present study, only specially orthotropic VAT laminates are considered. In other words, there are no in-plane and out-of-plane couplings ($\boldsymbol{B}=0$), no extension-shear coupling ($A_{16}=0, A_{26}=0$), and no flexural-twisting coupling ($D_{16}=0$, $D_{26}=0$). As a result, two in-plane and two out-of-plane lamination parameters are sufficient to define the stiffness matrices as

$$\begin{pmatrix} A_{11} \\ A_{22} \\ A_{12} \\ A_{66} \end{pmatrix} = h \begin{bmatrix} 1 & \xi_1^A & \xi_2^A & 0 & 0 \\ 1 & -\xi_1^A & \xi_2^A & 0 & 0 \\ 0 & 0 & -\xi_2^A & 1 & 0 \\ 0 & 0 & -\xi_2^A & 0 & 1 \end{bmatrix} \begin{pmatrix} U_1 \\ U_2 \\ U_3 \\ U_4 \\ U_5 \end{pmatrix} \tag{2}$$

$$\begin{pmatrix} D_{11} \\ D_{22} \\ D_{12} \\ D_{66} \end{pmatrix} = \frac{h^3}{12} \begin{bmatrix} 1 & \xi_1^D & \xi_2^D & 0 & 0 \\ 1 & -\xi_1^D & \xi_2^D & 0 & 0 \\ 0 & 0 & -\xi_2^D & 1 & 0 \\ 0 & 0 & -\xi_2^D & 0 & 1 \end{bmatrix} \begin{pmatrix} U_1 \\ U_2 \\ U_3 \\ U_4 \\ U_5 \end{pmatrix} \tag{3}$$

where the four lamination parameters are defined by

$$\begin{aligned} \xi_{1,2}^A &= \frac{1}{2}\int_{-1}^{1} [\cos(2\theta(\bar{z}))\cos(4\theta(\bar{z}))]\mathrm{d}\bar{z} \\ \xi_{1,2}^D &= \frac{3}{2}\int_{-1}^{1} [\cos(2\theta(\bar{z}))\cos(4\theta(\bar{z}))]\mathrm{d}\bar{z} \end{aligned} \tag{4}$$

where $\theta(\bar{z})$ is the layup function in the thickness direction of the plate.

B. Feasible Region of Lamination Parameters

The entire distribution of spatial variable stiffness of the VAT laminates are not independent of each other; and their feasible region, in terms of lamination parameters, forms a convex space [19]. Their values are required to be strictly constrained inside the feasible region to ensure a stable optimization procedure for the design of VAT laminates. An accurate boundary of the feasible region of lamination parameters is then important for the optimization of VAT laminates. Grenestedt and Gudmindson [19] presented a set of equations that gave an outer boundary for the feasible region of lamination parameters. In the current work, we derive a set of new explicit closed-form expressions that accurately defines the interdependent feasible region of $\xi_{1,2}^A$ and $\xi_{1,2}^D$. The derivation of these equations is given in Appendix A. The nonlinear constraints for these four coupled lamination parameters are given by

$$5(\xi_1^A - \xi_1^D)^2 - 2(1 + \xi_2^A - 2(\xi_1^A)^2) \le 0 \tag{5}$$

$$(\xi_2^A - 4t\xi_1^A + 1 + 2t^2)^3 - 4(1+2|t|+t^2)^2(\xi_2^D - 4t\xi_1^D + 1 + 2t^2) \le 0 \tag{6}$$

$$(4t\xi_1^A - \xi_2^A + 1 + 4|t|)^3 - 4(1+2|t|+t^2)^2(4t\xi_1^D - \xi_2^D + 1 + 4|t|) \le 0 \tag{7}$$

where $t = [-1, -0.75, -0.5, -0.25, 0, 0.25, 0.5, 0.75, 1]$ (or, for better accuracy, $t = [-1, -0.8, -0.6, -0.4, -0.2, 0, 0.2, 0.4, 0.6, 0.8, 1]$). These $19 \sim 23$ equations in Eqs. (5–7) are able to accurately bound the feasible region of the four lamination parameters ($\xi_{1,2}^{A,D}$), as shown in Fig. A2.

III. Buckling Analysis

Before buckling analysis, the nonuniform load redistribution of in-plane stress resultants of VAT plates that arises in response to stiffness variations is required [2,38]. Here, both the prebuckling and buckling problems are solved using a Rayleigh–Ritz procedure through the minimization of potential energy (or complementary energy).

To take advantage of the linear relations, as shown in Eqs. (2) and (3), between the stiffness matrices (A, D) and the lamination parameters ($\xi_{1,2}^{A,D}$), the VAT plate is modeled in terms of displacement fields, each of which is expanded into an independent series:

$$u^0(x,y) = \sum_{p}^{P_1}\sum_{q}^{Q_2} U_{pq} X_p^u(x) Y_q^u(y),$$
$$v^0(x,y) = \sum_{p}^{P_2}\sum_{q}^{Q_2} V_{pq} X_p^v(x) Y_q^v(y),$$
$$w(x,y) = \sum_{m}^{M}\sum_{n}^{N} W_{mn} X_m^w(x) Y_n^w(y) \tag{8}$$

where U_{pq}, V_{pq}, and W_{mn} are undetermined coefficients for three displacement components $u^0(x,y)$, $v^0(x,y)$, and $w(x,y)$, respectively. The shape functions $X_p^u(x), Y_q^u(x), \cdots, Y_n^w(x)$ in the series expansions must satisfy geometric boundary conditions on the edges.

By substituting the series expansions of $u^0(x,y)$ and $v^0(x,y)$ in Eq. (8) into the potential energy, the in-plane stretching problem of VAT plates under a prescribed force loading is solved and given by [39,40] as

$$\Pi_s = \frac{1}{2}\int\int\left[A_{11}\left(\frac{\partial u^0}{\partial x}\right)^2 + 2A_{12}\left(\frac{\partial u^0}{\partial x}\frac{\partial v^0}{\partial y}\right) + A_{22}\left(\frac{\partial v^0}{\partial x}\right)^2 + A_{66}\left(\frac{\partial u^0}{\partial y} + \frac{\partial v^0}{\partial x}\right)^2\right]\mathrm{d}x\,\mathrm{d}y - \int_{C_1}(\bar{N}_{xv}u + \bar{N}_{yv}v)\mathrm{d}s \tag{9}$$

where $\bar{N}_{xv}$ and $\bar{N}_{yv}$ are in-plane boundary stress resultants. The prebuckling problem of a VAT plate under prescribed loading is modeled as a linear algebraic problem, which is expressed in matrix form as

$$K^m \cdot \boldsymbol{U} = \boldsymbol{F} \tag{10}$$

where $\boldsymbol{U}$ is a vector of the undetermined coefficients ($[\,U_{pq} \quad V_{pq}\,]^T$) from the in-plane displacement fields $u^0(x,y)$ and $v^0(x,y)$. The vector $\boldsymbol{F}$ is associated with the prescribed in-plane loading. Note that, using Eq. (10) to directly model a VAT plate subjected to prescribed displacement boundary conditions $\boldsymbol{u}_0$ (i.e., an end-shortening displacement compression), is generally difficult to achieve, as the boundary forces are nonuniform and unknown [38]. As prebuckling is a linear elasticity problem, the superposition principle is applied. As such, the prebuckling problem of a VAT plate under a prescribed displacement loading $\boldsymbol{u}_0$ is modeled as a superposition of the VAT plates under a series of given nonuniform boundary stress loading conditions. Equation (10) is then rewritten as

$$K^m \cdot \boldsymbol{U}_j = \boldsymbol{F}_j \tag{11}$$

where the vector $\boldsymbol{F}_j$ denotes applied boundary force, which is assumed to be constant, linear, parabolic, cubic, and higher-order variations for $\boldsymbol{j} = 0, 1, 2, \cdots$. The prebuckling model of a VAT plate under prescribed displacement loading is then expressed as a sum of a series of the solution of Eq. (11) with undetermined weights c_j:

$$\sum_j c_j(K^m \cdot \boldsymbol{U}_j) = \sum_j c_j \boldsymbol{F}_j \Rightarrow \quad K^m \cdot \sum_j c_j \boldsymbol{U}_j = \sum_j c_j \boldsymbol{F}_j \tag{12}$$

where the coefficients c_j are determined by satisfying the boundary conditions $\boldsymbol{u}_0$

$$\left[\sum_j c_j \boldsymbol{U}_j\right] \cdot \boldsymbol{\psi}(\boldsymbol{x})|_{x=x_j} = \boldsymbol{u}_0 \tag{13}$$

and $\boldsymbol{\psi}(\boldsymbol{x})$ denotes a vector of in-plane shape functions $[X_p^u(x)Y_q^u(y)]^T$ (or $[X_p^v(x)Y_q^v(y)]^T$), and $\boldsymbol{x}_j = (x_j, y_j)$ is a selected grid point along the boundary edges where the boundary conditions $\boldsymbol{u}_0$ are applied. Subsequently, the nonuniform stress fields are obtained from the constitutive equation as

$$\boldsymbol{N} = A \cdot \epsilon^0 = A \cdot D\boldsymbol{u}(\boldsymbol{x}) = A \cdot [D\boldsymbol{\psi}(\boldsymbol{x})] \cdot \sum_j c_j \boldsymbol{U}_j \tag{14}$$

By substituting the transverse deflection $w(x,y)$ into the potential energy for bending of VAT plates [38], the buckling analysis is expressed as the following eigenvalue problem:

$$\{[K^b] - \lambda[K^s]\}\{\boldsymbol{w}\} = 0 \tag{15}$$

Note that different approaches (finite element method, the finite difference method, and differential quadrature method [41]) have been used to model the prebuckling and buckling behaviors of VAT plates, resulting in the same matrix formulas as Eqs. (11) and (15). The optimization methodologies presented in subsequent sections are applicable to other modeling approaches. Of these, the Rayleigh–Ritz (or Galerkin) method has the advantage that it requires relatively little computational cost and allows sensitivities to be calculated analytically.

IV. Two-Level Optimization Strategy

The buckling optimization procedure of VAT plates is split into two steps. At the first step, a gradient-based mathematical programming technique is used to determine the optimum distribution/variation of lamination parameters, which gives the maximum buckling load. At the second step, a GA is employed as an optimizer to obtain the actual layups (stacking sequence and fiber orientations) from the target value of lamination parameters.

A. First-Level Optimization

1. *B-Spline Spatial Variation of Lamination Parameters*

The distribution of four lamination parameters ($\xi_{1,2}^{A,D}$) for establishing an orthotropic VAT laminate configuration is represented in terms of the B-spline surface as

$$x(\bar{u},\bar{v}) = \sum_r\sum_s B_{rs}^{(x)} N_r^{(k)}(\bar{u}) N_s^{(k)}(\bar{v})$$
$$y(\bar{u},\bar{v}) = \sum_r\sum_s B_{rs}^{(y)} N_r^{(k)}(\bar{u}) N_s^{(k)}(\bar{v})$$
$$\xi_{1,2}^{A,D}(\bar{u},\bar{v}) = \sum_r\sum_s \Gamma_{rs}^{(\tau)} N_r^{(k)}(\bar{u}) N_s^{(k)}(\bar{v}) \tag{16}$$

where the values of $B_{rs}^{(x)}$ and $B_{rs}^{(y)}$ represent the location of each predefined control point P_{rs} (as shown in Fig. 1) along the x and y axes, respectively. The coefficient $\Gamma_{rs}^{(\tau)}$ in Eq. (16) is the assigned value of a particular lamination parameter at each predefined control point (P_{rs}). The term $\tau = 1, 2, 3$, and 4 denotes four different lamination parameters ξ_1^A, ξ_2^A, ξ_1^D, and ξ_2^D, respectively. The B-spline basis function $N_r^{(k)}(\bar{u})$ [or $N_s^{(k)}(\bar{v})$] is a kth order ($k-1$ degree) piecewise polynomial that is determined by a defined knot vector Ξ. When the lamination parameters (stiffness) are defined to vary along one principal direction (for example, the y axis), the variation is defined by the B-spline curve:

$$y(\bar{v}) = \sum_s B_s^{(y)} N_s^{(k)}(\bar{v}) \quad \xi_{1,2}^{A,D}(\bar{v}) = \sum_s \Gamma_s^{(\tau)} N_s^{(k)}(\bar{v}) \tag{17}$$

Figure 1 demonstrates an example of using the B-spline surface with 5-by-5 (25) uniformly spaced control points to construct the distribution of lamination parameters varying along both the x and y axes. The order and the knot vector for the B-splines in this example

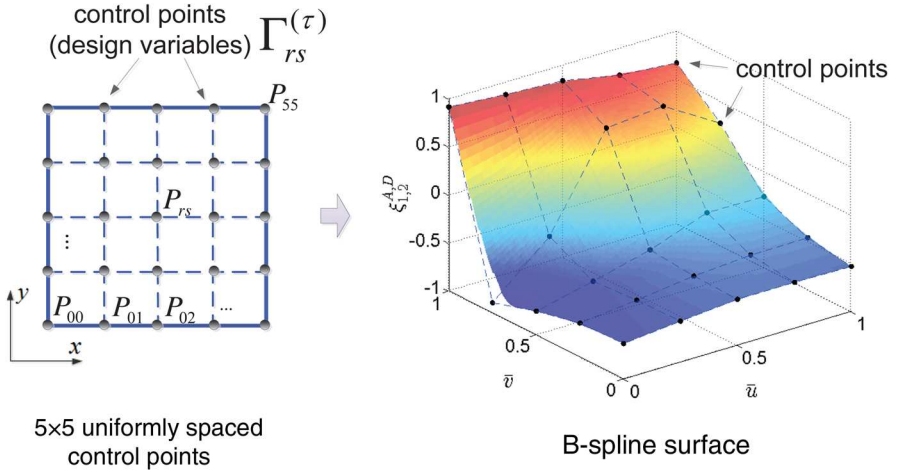

Fig. 1 Illustration of B-spline surface constructing by five-by-five uniformly spaced control points.

are chosen to be $k = 3$ and $\Xi = [0, 0, 0, 1/3, 2/3, 1, 1, 1]$ (uniform), respectively. Figure 2 shows the open uniform B-spline basis functions, which are piecewise quadratic polynomials. The optimal design is performed by adjusting the values of the lamination parameters ($\xi_{1,2}^{A,D}$) at the 25 control points, and this approximation does not represent the complete design space. However, increasing the number of control points ensures greater convergence of the complete design space.

B-splines possess several special features, which make them suitable for representing the spatial variation of lamination parameters of VAT laminates. Using B-splines generally results in continuous and smooth distributions, with the degree of local variation specified by k. The plate domain is subdivided into a grid that consists of a series of patches, and the B-splines are defined locally over each patch. The local support property of B-spline controls the variation within each patch, i.e., adjusting the value of a control point only affects variation inside the local patch. This feature is particularly useful for the concept of local stiffness tailoring and offers the possibility of implementing a tool for both modeling and optimization of blended VAT laminates. Another desirable feature of B-splines is their strong convex hull property, which states that a B-spline surface is strictly constrained in the convex hull formed by its control polygon. This convex hull property enables the entire distribution of the lamination parameters to be constrained strictly inside the feasible region by satisfying the nonlinear constraints defined in Eqs. (5–7) at the control points. Using other algebraic polynomial functions (but without the convex hull property) leads to a semi-infinite programming problem in the optimization of VAT laminates. Solving a semi-infinite programming problem is highly computationally expensive and may cause the optimization procedure to be numerically unstable.

Using higher-degree B-spline basis functions [for instance, the cubic variation ($k = 4$)] offers more local flexibility for the design of variable stiffness. However, it also limits the usage of design space compared to quadratic variation. Applying the nonuniform rational B-splines to represent the variation of lamination parameters provides larger design space and more design options (local refinement) than using the B-splines, as NURBS introduces a weighting coefficient (four-dimensional space) to each control point. However, the NURBS-based approach may considerably raise the difficulty of evaluating the sensitivities and the computational cost of optimization. As the plane domain of a VAT plate is smoothly varying, it is appropriate to use uniform basis functions and uniform-spaced control points to represent its stiffness variation. We anticipate that nonuniform basis functions and control points are better suited for the design of VAT laminates with cutouts and discontinuities.

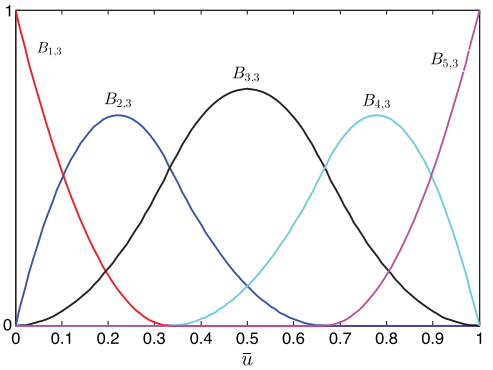

Fig. 2 Uniform B-spline basis functions for $N = 5$, $k = 3$ and $\Xi = [0,0,0,1/3,2/3,1,1,1]$.

As the stiffness variation (lamination parameters) of VAT plates is defined in a B-spline parametric space $(\bar{u}, \bar{v})$ [Eq. (16)], all the integrations involved in the prebuckling and buckling models [Eqs. (11–15)] defined over the plate domain (x, y) have to be transformed and evaluated in the B-Spline parametric domain. For example,

$$\int_{\Omega} A_{11}(x,y)\cdot\Psi(x,y)\,\mathrm{d}x\,\mathrm{d}y = \int_{\Omega^*} A_{11}(\bar{u},\bar{v}) \cdot \Psi(x(\bar{u},\bar{v}),y(\bar{u},\bar{v}))J_{\bar{u}\bar{v}}\,\mathrm{d}\bar{u}\,\mathrm{d}\bar{v} \tag{18}$$

where $\Psi(x, y)$ denotes a shape function that is employed in the model. The terms Ω and Ω^* represent the integral domain under (x, y) and $(\bar{u}, \bar{v})$ coordinates, respectively; and $J_{\bar{u}\bar{v}}$ is the Jacobian matrix for the coordinates transformation. Equation (18) is further expanded in terms of lamination parameters as

$$\int_{\Omega^*} A_{11}(\bar{u},\bar{v})\cdot\tilde{\Psi}(\bar{u},\bar{v})J_{\bar{u}\bar{v}}\mathrm{d}\bar{u}\,\mathrm{d}\bar{v} = h\left[U_0\int_{\Omega^*}\tilde{\Psi}(\bar{u},\bar{v})J_{\bar{u}\bar{v}}\mathrm{d}\bar{u}\,\mathrm{d}\bar{v} + \sum_{rs}(U_1\Gamma_{rs}^{(1)}+U_2\Gamma_{rs}^{(2)})\int_{\Omega^*}N_r^{(k)}(\bar{u})N_s^{(k)}(\bar{v})\tilde{\Psi}(\bar{u},\bar{v})J_{\bar{u}\bar{v}}\mathrm{d}\bar{u}\,\mathrm{d}\bar{v}\right] \tag{19}$$

On the right-hand side of Eq. (19), the integrals are independent of material properties, plate dimensions, and the design variables ($\Gamma_{rs}^{(1)}$, $\Gamma_{rs}^{(2)}$). All of the other integrations in the prebuckling and buckling models are also transformed and expanded in a similar way to Eqs. (18) and (19). The numerical computation of these integrals, which is the most time consuming of the proposed design framework but only needs to be performed once in the whole optimization process. Furthermore, due to the local support property of B-spline basis function, $N_r^{(k)}(\bar{u})$ and $N_s^{(k)}(\bar{v})$ are nonzero only at a local region $[t_r, t_{r+k}]$ ($[t_s, t_{s+k}]$). Each individual integration, for example,

$$\int_{\Omega^*} N_r^{(k)}(\bar{u})N_s^{(k)}(\bar{v})\tilde{\Psi}(\bar{u},\bar{v})J_{\bar{u}\bar{v}}\,\mathrm{d}\bar{u}\,\mathrm{d}\bar{v} = \int_{t_r}^{t_{r+k}}\int_{t_s}^{t_{s+k}} N_r^{(k)}(\bar{u})N_s^{(k)}(\bar{v})\tilde{\Psi}(\bar{u},\bar{v})J_{\bar{u}\bar{v}}\,\mathrm{d}\bar{u}\,\mathrm{d}\bar{v} \tag{20}$$

is evaluated over a local B-spline patch.

2. Sensitivity

The numerical accuracy of sensitivity information plays an important role in a gradient-based optimization routine. The buckling analysis of VAT plates is a conventional eigenvalue problem, and the sensitivity of the critical buckling load with respect to each design variable (lamination parameters at each control point) is evaluated as [42]

$$\frac{\mathrm{d}\lambda}{\mathrm{d}\Gamma_{rs}^{(\tau)}} = \left[\boldsymbol{w}^T \left(\frac{\mathrm{d}K^b}{\mathrm{d}\Gamma_{rs}^{(\tau)}} - \lambda \frac{\mathrm{d}K^s}{\mathrm{d}\Gamma_{rs}^{(\tau)}} \right) \boldsymbol{w} \right] \tag{21}$$

where the buckling mode shape is normalized as $\boldsymbol{w}^T K^s \boldsymbol{w} = 1$. As illustrated by Eq. (19), the matrices (K^b and K^s) are separable with respect to design variables (lamination parameters). Hence, the matrices K^b and K^s are further expanded and written in the following form:

$$K^b = K_0^b + \sum_{rs} \Gamma_{rs}^{(3)} K_1^b + \sum_{rs} \Gamma_{rs}^{(4)} K_2^b \tag{22}$$

$$\begin{aligned} K^s = {} & \sum_{pq} U_{pq} K_{10}^s + \sum_{pq} \sum_{rs} U_{pq} \Gamma_{rs}^{(1)} K_{11}^s + \sum_{pq} \sum_{rs} U_{pq} \Gamma_{rs}^{(2)} K_{12}^s \\ & + \sum_{pq} V_{pq} K_{20}^s + \sum_{pq} \sum_{rs} V_{pq} \Gamma_{rs}^{(1)} K_{21}^s + \sum_{pq} \sum_{rs} V_{pq} \Gamma_{rs}^{(2)} K_{22}^s \end{aligned} \tag{23}$$

where $K_0^b, K_1^b, \cdots, K_{22}^s$ on the right-hand side of Eq. (23) are the separated parts of the stiffness and stability matrices, which are functions of material invariants and B-splines (at each control point). In Eq. (22), the matrix K_0^b is independent of design variables. The matrices K_1^b and K_2^b are related to the out-of-plane lamination parameters of ξ_1^D and ξ_2^D at each control point (P_{rs}), respectively.

The stability matrix K^s is related to both in-plane lamination parameters and in-plane displacement fields $[U_p, V_p]^T$ (prebuckling solution). For the matrices $K_{10}^s, K_{11}^s, \cdots, K_{22}^s$ in Eq. (23), the number in their subscripts $(10, 11, \cdots, 22)$ specifies the relation of the corresponding matrix to the design variables and in-plane displacement fields. The first index in each subscript (1 or 2) indicates that the matrix is associated with u^0 or v^0 displacement fields. The second index (0, 1, 2) in each subscript denotes the corresponding matrix is independent of design variables (equal to zero), associated with ξ_1^A (equal to one) and ξ_2^A (equal to two), respectively. All of the explicit expressions of these matrices in the Appendix B.

As previously mentioned, in Eqs. (22) and (23), the integrals involved in $K_0^b, K_1^b, \cdots, K_{22}^s$ are independent of the design variables and are only evaluated once in an optimization process. The sensitivities in Eq. (21) are computed analytically based on the value of these matrices, and so improve the efficiency of the gradient-based optimization process. Due to the linear relationship between the bending stiffness matrix and the out-of-plane lamination parameters, the derivative of K^b in Eq. (21) is evaluated separately as

$$\frac{\mathrm{d}K^b}{\mathrm{d}\Gamma_{rs}^{(3)}} = K_1^b, \qquad \frac{\mathrm{d}K^b}{\mathrm{d}\Gamma_{rs}^{(4)}} = K_2^b \tag{24}$$

On the other hand, a local change of in-plane stiffness may affect the entire in-plane stress distribution (prebuckling solution) [5]. The sensitivity evaluation of the stability matrix K^s is related (coupled) to each component (U_p, V_p) of the series expansion of the in-plane displacement field as

$$\begin{aligned} \frac{\mathrm{d}K^s}{\mathrm{d}\Gamma_{rs}^{(1)}} = {} & \sum_{pq} \left[\frac{\mathrm{d}U_{pq}}{\mathrm{d}\Gamma_{rs}^{(1)}} K_{10}^s + \frac{\mathrm{d}U_{pq}}{\mathrm{d}\Gamma_{rs}^{(1)}} \Gamma_{rs}^{(1)} K_{11}^s + U_{pq} K_{11}^s + \frac{\mathrm{d}U_{pq}}{\mathrm{d}\Gamma_{rs}^{(1)}} \Gamma_{rs}^{(2)} K_{12}^s \right] \\ & + \sum_{pq} \left[\frac{\mathrm{d}V_{pq}}{\mathrm{d}\Gamma_{rs}^{(1)}} K_{20}^s + \frac{\mathrm{d}V_{pq}}{\mathrm{d}\Gamma_{rs}^{(1)}} \Gamma_{rs}^{(1)} K_{21}^s + V_{pq} K_{21}^s + \frac{\mathrm{d}V_{pq}}{\mathrm{d}\Gamma_{rs}^{(1)}} \Gamma_{rs}^{(2)} K_{22}^s \right] \end{aligned} \tag{25}$$

$$\begin{aligned} \frac{\mathrm{d}K^s}{\mathrm{d}\Gamma_{rs}^{(2)}} = {} & \sum_{pq} \left[\frac{\mathrm{d}U_{pq}}{\mathrm{d}\Gamma_{rs}^{(2)}} K_{10}^s + \frac{\mathrm{d}U_{pq}}{\mathrm{d}\Gamma_{rs}^{(2)}} \Gamma_{rs}^{(1)} K_{11}^s + U_{pq} K_{12}^s + \frac{\mathrm{d}U_{pq}}{\mathrm{d}\Gamma_{rs}^{(2)}} \Gamma_{rs}^{(2)} K_{12}^s \right] \\ & + \sum_{pq} \left[\frac{\mathrm{d}V_{pq}}{\mathrm{d}\Gamma_{rs}^{(2)}} K_{20}^s + \frac{\mathrm{d}V_{pq}}{\mathrm{d}\Gamma_{rs}^{(2)}} \Gamma_{rs}^{(1)} K_{21}^s + V_{pq} K_{22}^s + \frac{\mathrm{d}V_{pq}}{\mathrm{d}\Gamma_{rs}^{(2)}} \Gamma_{rs}^{(2)} K_{22}^s \right] \end{aligned} \tag{26}$$

The derivatives of the in-plane displacement fields $\boldsymbol{U}([\,U_p \quad V_p\,]^T)$ are determined from the prebuckling model as

$$\frac{\mathrm{d}\boldsymbol{U}}{\mathrm{d}\Gamma_{rs}^{(\tau)}} = \sum_j \left[\frac{\mathrm{d}c_j}{\mathrm{d}\Gamma_{rs}^{(\tau)}} \boldsymbol{U}_j + c_j \frac{\mathrm{d}\boldsymbol{U}_j}{\mathrm{d}\Gamma_{rs}^{(\tau)}} \right] \qquad (\tau = 1, 2) \tag{27}$$

$$\frac{\mathrm{d}c_j}{\mathrm{d}\Gamma_{rs}^{(\tau)}} = -(\boldsymbol{U}_0)^{-1} \frac{\mathrm{d}\boldsymbol{U}_0}{\mathrm{d}\Gamma_{rs}^{(\tau)}} [c_j] \qquad (\tau = 1, 2) \tag{28}$$

$$\frac{\mathrm{d}\boldsymbol{U}_j}{\mathrm{d}\Gamma_{rs}^{(\tau)}} = -(K^m)^{-1} \frac{\mathrm{d}K^m}{\mathrm{d}\Gamma_{rs}^{(\tau)}} \boldsymbol{U}_j \qquad (\tau = 1, 2) \tag{29}$$

where $\boldsymbol{U}_0$ denotes the expression for $\boldsymbol{\psi}(\boldsymbol{x})\boldsymbol{U}^{(k)}|_{x=x_0}$.

Besides the sensitivities of buckling load, it is also necessary to obtain the gradient information of the nonlinear constraint functions (feasible region of lamination parameters), which is done readily from the expressions given in Eqs. (5–7).

3. Gradient-Based Optimization

The buckling load of a VAT plate is a function of both in-plane stiffness and bending stiffness $\lambda_{\mathrm{cr}} = \lambda(A, D)$ [2,3] due to the nonuniform in-plane stress fields. It was observed that the buckling load is a linear homogeneous function with respect to the bending stiffness. The in-plane stresses are linear functions of the reciprocal of the in-plane compliance A^{-1} and proportional to the external applied boundary force (displacement) [3]. Also, varying the amplitude of in-plane stresses does not affect the buckling eigenvalue (zero-order homogeneous property [5]), and only the stress distribution affects the buckling load. Therefore, the in-plane stiffness of VAT laminates has to be optimized to achieve a benign stress distribution that improves their buckling performance [2,3,5].

From our physical understanding, the improvement in buckling performance is mainly governed by the stress redistribution of loads from the center to the edges where the plate is supported. For straight fiber composites, the sensitivity of curvature plays a prominent role in improving the buckling performance, as it is governed by bending action of the plate. However, for VAT laminates, the buckling performance is governed by both stretching and bending behaviors. For VAT plates that are under axial compression loading conditions, the sensitivity of strains at both the domain and the boundary is equally important in redistributing the loads from the center toward the supported edges.

The sensitivity analysis [Eqs. (21–28)] shows that the buckling load is nonlinear with respect to each component of the in-plane stiffness matrix A_{ij}. The distributions of in-plane stiffness and the bending stiffness cannot vary independently and are linked by the values of material invariants and lamination parameters in a convex feasible space. Hence, the buckling design of VAT plates is a coupled nonlinear optimization problem in terms of stiffness matrices expressed using lamination parameters and requires nonlinear constraints to define the feasible region of lamination parameters. The first-level optimization of VAT plates for the maximum buckling load using lamination parameters is formulated as

$$\min \quad -\lambda_{\mathrm{cr}}(\Gamma_{rs}^{(\tau)}) \quad \text{subjected to :} \quad -1 \leqslant \Gamma_{rs}^{(\tau)} \leqslant 1 \quad g_i(\Gamma_{rs}^{(\tau)}) \leqslant 0 \tag{30}$$

The nonlinear constraint functions $g_i(\Gamma_{rs}^{(\tau)})$ define the relations between the four different lamination parameters, given by

Eqs. (5–7). The satisfaction of the nonlinear constraints (feasible region) in $g_i(\Gamma_{rs}^{(\tau)})$ for the lamination parameters is crucial in the optimization process. The failure to satisfy the feasibility constraints by the lamination parameter distributions may either lead to an unstable optimization process or an infeasible solution.

In a GCMMA approach, approximation of the objective function and nonlinear constraints in a local region is shown to be convex separable and conservative with respect to each design variable (lamination parameters). The approximation function is constructed based on the gradient information computed from the buckling model [Eq. (15)] and sensitivity analysis [Eqs. (22–28)]. In a GCMMA scheme, the buckling load factor and the nonlinear constraints in Eq. (30) are approximated in convex separable forms as [26]

$$\bar{f}_i^{(\mu,\nu)}(\mathbf{\Gamma}) = \sum_{j=1}^{n}\left(\frac{p_{ij}^{(\mu,\nu)}}{\alpha_j^{(\mu)} - \Gamma_j} + \frac{q_{ij}^{(\mu,\nu)}}{\Gamma_j - \beta_j^{(\mu)}}\right) + r_i^{(\mu,\nu)} \tag{31}$$

where μ and ν denote the indices of the "outer" and "inner" iterations, respectively. For the detailed expression of each variable in Eq. (31), refer to [26]. The terms $\alpha_j^{(\mu)}$ and $\beta_j^{(\mu)}$ are the upper and lower moving asymptotes, respectively. For each design variable, the values of $p_{ij}^{(\mu,\nu)}$ and $q_{ij}^{(\mu,\nu)}$ are associated with the positive and negative sensitivities, as well as the upper and lower moving asymptotes, respectively. The difference between the objective function and the approximation formula for the original design when each outer iteration begins is denoted by $r_i^{(\mu,\nu)}$. Additional damping factors are introduced in the expressions of $p_{ij}^{(\mu,\nu)}$, $q_{ij}^{(\mu,\nu)}$, and $r_i^{(\mu,\nu)}$ for strictly ensuring the convexity and conservativeness of the approximating formula. As such, at a local design region, the objective function in Eq. (30) is replaced by Eq. (31), which can be solved through a dual method [26,32]. IJsselmuiden et al. [5] used a simplified expression in terms of in-plane stiffness, and the inverse bending stiffness matrices (mixed-variable approach) is proposed for the buckling optimization, in which the advantage of homogeneous properties of the buckling model of variable stiffness laminate is taken. Equation (31) is a general approximating scheme that constructs convex subproblems based on gradient information and the corresponding curvatures (asymptotes) and damping factors. This approach is general and suitable for other optimization problems (e.g., postbuckling).

In a GCMMA routine, at each outer iteration, the buckling load and sensitivities are computed and a suboptimization problem is generated based on Eq. (30). Suboptimization problems are then solved iteratively by updating the damping factors until a complete conservativeness is achieved (inner iteration). The conservativeness check ensures the lamination parameter distributions are strictly constrained inside the feasible region, which leads to a stable and fast convergent optimization procedure. As the objective function in terms of lamination parameters is well conditioned and Eq. (31) is a convex approximation, it typically requires only a few iterations to solve a subproblem. Therefore, the entire process of the first-level buckling optimization of VAT plates is performed with appropriate accuracy and efficiency.

B. Second-Level Optimization

The objective of the second-level optimization process is to retrieve a realistic VAT layup that can approximately give the same lamination parameters distribution as the optimal results. For a VAT layup, the stacking arrangement and spatial variation of fiber angles for each layer is required. The relationship between lamination parameters and stacking sequence is not unique and is complicated [8], partially due to the nonbijective relationship and due to conversion from a continuous to a discrete problem. Hence, it is not always possible to directly convert the optimal lamination parameters into realistic layups using explicit formulas. To accomplish this task, a VAT lamination configuration that can closely match the target lamination parameters is sought using a genetic algorithm.

Here, an antisymmetrical stacking sequence with specially orthotropic properties ($[B] = 0, A_{16}, A_{26} = 0, D_{16}, D_{26} = 0$) is extensively used as a test laminate. For example, the stacking sequence of a 16-layer laminate is $[\pm\theta_1/\mp\theta_1/\pm\theta_2/\mp\theta_2]_{AS}$, which possesses two VAT design layers; and $\theta_1(x, y)$, $\theta_2(x, y)$ captures specially orthotropic properties. The design flexibility for the through-the-thickness stacking rearrangement can be extended by increasing the number of design layers. For each VAT layer, the spatially varying fiber-orientation angles are described by a general definition for the nonlinear continuous variation of fiber-orientation angles. The nonlinear variation (NLV) of fiber orientations is defined based on a set of $M_1 \times N_1$ preselected control points in the plate domain, as illustrated in Fig. 3. Lagrangian polynomials are used to interpolate the prescribed fiber angles at the control points and construct a nonlinear distribution of fiber angles, given by the following series form [3]:

$$\theta(x, y) = \sum_{m=0}^{M_1-1}\sum_{n=0}^{N_1-1} T_{mn} \cdot \prod_{m\neq i}\left(\frac{x - x_i}{x_m - x_i}\right) \cdot \prod_{n\neq j}\left(\frac{y - y_j}{y_n - y_j}\right) \tag{32}$$

where the advantage of this formulation is that the coefficient of each term (T_{mn}) in Eq. (32) directly equals the value of fiber angle at a specific control point (x_m, y_n). This formulation parameterizes each VAT layer in terms of a small number of fiber-orientation angles at the preselected control points. We observed that, for a flat VAT plate, three to five grid points along each direction are usually sufficient to obtain converged fiber angle distribution results. In addition, this formulation gives a continuous, smooth distribution for the fiber orientations, which are suitable for conversion into practical tow trajectories when the manufacturing constraints are considered. Figure 3 demonstrates two VAT configurations using three uniformly spaced control points along each direction.

In the second-level optimization process, a VAT laminate with a predefined number of layers and control points is first chosen, which represent the stacking sequence (number of design layers) and the control points (number and positions) for defining the nonlinear variation of fiber-orientation angles, respectively. Subsequently, a GA is used to determine the fiber-orientation angles at all of the control points within each design layer, which leads to the distribution of lamination parameters matching the desired continuous lamination parameter results as closely as possible.

For VAT plates, the fitness function is expressed as a mean value of the least-square distance between the obtained lamination parameters and the target lamination parameters evaluated at a large number of points in the plate [35]. The optimization problem is formulated as

$$\begin{aligned}
&\min\ \Delta\xi = \frac{1}{N_p}\sum_j \Delta\xi_j \\
&\Delta\xi_j = \left[\sum_i^2 w_i^A(\xi_i^A - \tilde{\xi}_i^A)^2 + \sum_i^2 w_i^D(\xi_i^D - \tilde{\xi}_i^D)^2\right]_{(j)} \\
&\xi_{1,2}^{A,D} \leftarrow [T_1^k, \cdots, T_n^k, \cdots, T_N^k] \\
&\text{subjected to: } -\pi/2 \leqslant T_n^k \leqslant \pi/2
\end{aligned} \tag{33}$$

where T_n^k is the fiber angle at the control point for the kth ply, and w_i^A and w_i^D are the weights to distinguish the relative importance between $\xi_{1,2}^A$ and $\xi_{1,2}^D$. The total number of grid points N_p is chosen to be $1000 \sim 2000$ in total for a two-dimensional variation. Based on our trial-and-error experiences, the population size was set to be at least $20 \sim 30$ times the number of design variables, whereas the number of generations is usually set to $50 \sim 100$, depending on the population size. The crossover and mutation probabilities were chosen to be 0.7 and 0.04. As the second-level optimization procedure is rapid, several trials can be carried out with different initial values, generation sizes, and population sizes to ensure that repeatable results are achieved.

As the objective function in Eq. (33) is not buckling-load-oriented (least-square-distance based), the optimization process may result in a local optimum with respect to the buckling load. The buckling load of the optimized VAT fiber angles from Eq. (33) is slightly lower (around $10 \sim 15\%$) than the target result given by the optimal lamination parameters. The fiber angles at the control points can be

$$\theta(x) = [T_0, T_1, T_2] \qquad \theta(x,y) = \begin{bmatrix} T_{00} & T_{01} & T_{02} \\ T_{10} & T_{11} & T_{12} \\ T_{20} & T_{21} & T_{22} \end{bmatrix}$$

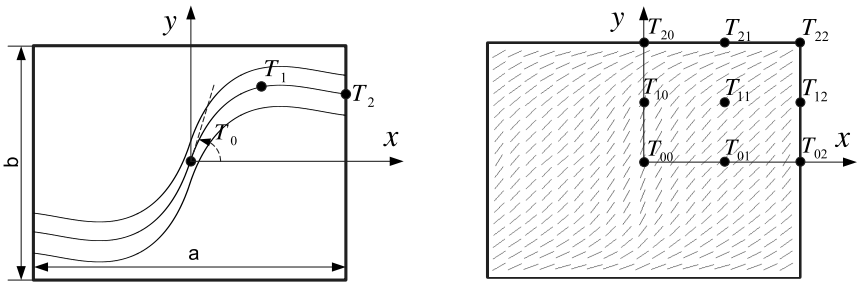

Fig. 3 Two illustrations for the nonlinear variation of fiber-orientation angles over the VAT plate domain. The fiber angles are parabolically varying along either x direction (left) or both axes directions (right).

further optimized by adding the buckling load as a sensitivity-based constraint [43,44]. A small number of iterations (less than 10) are able to yield a good VAT design that matches well with the global optimal solution from the first-level optimization process. Once a smooth distribution of nonlinear fiber-orientation angles is determined, it is straightforward to construct the manufacturable fiber (tow) trajectories. In future work, manufacturing and other design constraints will be considered in the second-level optimization process to generate manufacturable fiber courses.

V. Results and Discussion

This section presents the numerical results of the proposed two-level optimization strategy to design VAT plates for maximum buckling load. For a clear comparison, the material properties and the geometry of VAT plates in the present study are the same as previous works [1,2,5]. The lamina properties for the T300/5208 graphite–epoxy composite are $E_{11} = 181$ GPa, $E_{22} = 10.273$ GPa, $G_{12} = 7.1705$ GPa, and $\nu_{12} = 0.28$ [2]. The tow thickness is 0.127 mm. The thickness variation of a VAT plate due to the manufacture process is not considered in the present study, and the ply thickness is assumed to be constant. Two different in-plane boundary conditions for VAT plates under uniaxial displacement compression are studied, as illustrated in Fig. 4. The plate is subjected to uniform displacement compression ($x = \pm(a/2)$: $u = \mp(\Delta_x/2)$) and, in case A, the transverse edges are free to move (stress free, $N_{y0} = 0$); in case B, the transverse edges are constrained ($v = 0$).

To give a direct layup comparison, the buckling load of a VAT plate is normalized with respect to that of a homogeneous quasi-isotropic laminate [3]:

$$K_x = \frac{(\hat{N}_x^{\mathrm{cr}})_{\mathrm{vat}}}{(N_x^{\mathrm{cr}})_{\mathrm{iso}}} \tag{34}$$

where $(\hat{N}_x^{\mathrm{cr}})_{\mathrm{vat}}$ is the average compressive load:

$$(\hat{N}_x^{\mathrm{cr}})_{\mathrm{vat}} = \frac{1}{b}\int_{-\frac{b}{2}}^{\frac{b}{2}} N_x(y)\,\mathrm{d}y \tag{35}$$

and $(N_x^{\mathrm{cr}})_{\mathrm{iso}}$ is the critical buckling load of the quasi-isotropic laminate. The equivalent Young's modulus E_{iso}, Poisson's ratio ν_{iso}, and bending stiffness D_{iso} of the quasi-isotropic laminate are given by [35,45]

$$D_{\mathrm{iso}} = \frac{E_{\mathrm{iso}}h^3}{12(1-\nu_{\mathrm{iso}}^2)}, \quad \nu_{\mathrm{iso}} = \frac{U_4}{U_1}, \quad E_{\mathrm{iso}} = U_1(1-\nu_{\mathrm{iso}}^2) \tag{36}$$

A. Optimal Lamination Parameters (First Level)

1. *Square VAT Plates*

The two-level buckling optimization strategy presented is first applied to determine the optimal design for maximizing buckling performance of square VAT plates with all edges simply supported. The length and width of plate are $a = 0.254$ m and $b = 0.254$ m, respectively. This problem was also studied by Ijsselmuiden et al. [5] using a finite element-based design scheme. This section demonstrates the advantage of using B-splines to represent the variation of lamination parameters.

To examine the rate of convergence, the number of control points (in Fig. 5) is gradually increased from 5 to 11 along each direction. In

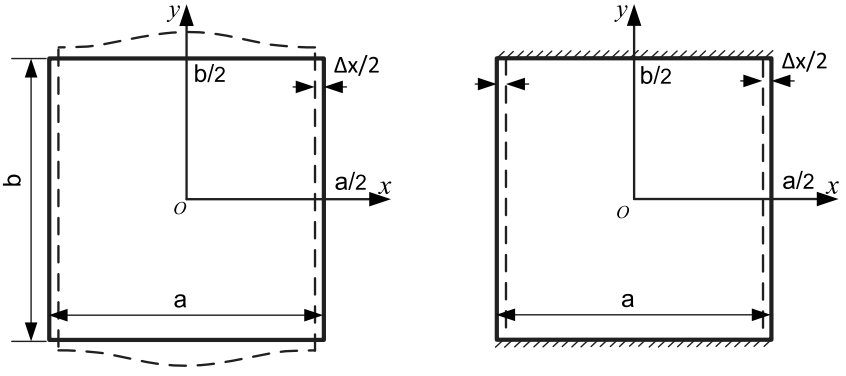

Fig. 4 Two cases of in-plane boundary conditions.

each optimization run, all the control points are uniformly distributed across the plate domain and uniform quadratic B-spline basis functions are used for constructing the variation of lamination parameters. The initial values of all lamination parameters at each control point are chosen to be zero, which corresponds to a quasi-isotropic layup. This also enables designers to compare the improvement in VAT laminate performance over a quasi-isotropic layup. Due to the symmetry of the buckling problem in terms of boundary conditions, geometry, and loadings, the lamination parameter distribution is designed to be doubly symmetric; that is, $\xi_{1,2}^{A,D}(x,y) = \xi_{1,2}^{A,D}(|x|,|y|)$. The control points for the B-splines that are used to define the lamination parameters distribution are shown in Fig. 1. The corresponding knot vectors are also chosen to be uniform as

$$\Xi_5 = [0,0,0,1/3,2/3,1,1,1],$$
$$\Xi_7 = [0,0,0,1/5,2/5,3/5,4/5,1,1,1],$$
$$\Xi_9 = [0,0,0,1/7,2/7,3/7,4/7,5/7,6/7,1,1,1],$$
$$\Xi_{11} = [0,0,0,1/9,2/9,3/9,4/9,5/9,6/9,7/9,8/91,1,1] \quad (37)$$

Table 1 lists the obtained maximum normalized buckling load K_{cr}^{*} using different numbers of control points, for both case A and case B. Besides the quasi-isotropic laminate, two layups ± 45 and $[\pm 36/\mp 36/\pm 24/\mp 24/0_4]_{AS}$ with maximum buckling loads among the constant-stiffness laminates (for each case) are also presented for comparison. The optimal normalized buckling loads of VAT plates are 2.9 and 2.0 for case A and case B, respectively, which indicates more than a 125 and 60% improvement of buckling resistance over the best layup of constant-stiffness laminates. It was observed that, for both cases, 7×7 control points for the B-splines to define the stiffness variation are sufficient to yield converged buckling optimization results. Figure 5 shows the convergence trends of the first-level optimization process for the boundary conditions of case A, using different numbers (5×5, 7×7, 9×9, and 11×11) of control points to construct the lamination parameter distributions. Correspondingly, the total number of design variables are 100, 196, 324, and 484. The computational expense for solving the modeling and optimization problem is only slightly increased with using more number of control points. Since the modeling (normally the most time-consuming part) is completely given by analytical formulations, the gradient-based routine only need spend few more internal iterations to complete the first-level optimization process.

All the control-point distributions exhibit rapid convergence within a few iterations (around 10). It is observed that, with an increase of the number of control points, a higher optimal buckling load is obtained. The curves for the 7×7, 9×9, and 11×11 control points are nearly coincident when the optimization process converges. This also shows that the full design space can be achieved approximately by increasing the number of control points. The optimal variations (7×7 control points) of the four lamination parameters are plotted in Fig. 6, for both cases. The contour plots of the

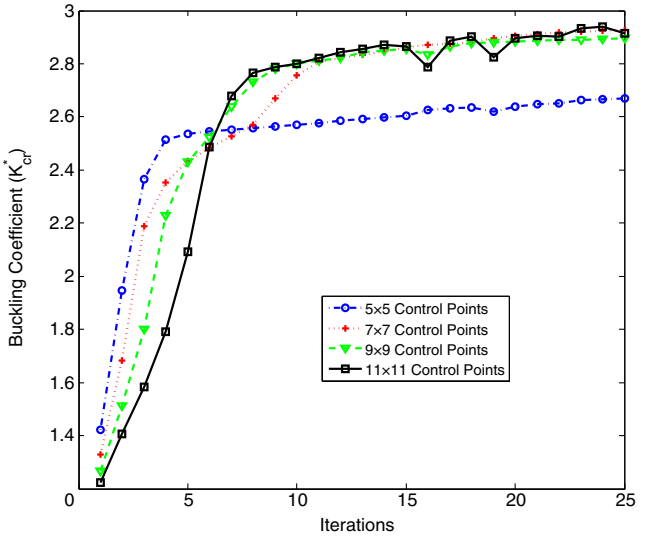

Fig. 5 Convergence trends of the first-level optimization process using different numbers of control points for constructing the B-spline form variation of lamination parameters along the *y* axis.

lamination parameters in Fig. 6 exhibit smoothness without notable discontinuity and match well with the results obtained by Ijsselmuiden et al. [5]. However, in the present approach, the number of design variables (196) for achieving convergent optimal results is much less than that (1764) of the finite element approach [5].

Figure 7 illustrates the in-plane stress distributions (N_x, N_y, N_{xy}) of the VAT plate with optimal lamination parameter distribution for the maximum buckling load (both case A and case B). It demonstrates that the load redistribution (toward the supported edges) induced by variable stiffness is the main contributing factor to improve the buckling resistance of VAT laminates. It is also interesting to note that a VAT plate subjected to uniaxial compression gives rise to a small amount of internal shear stresses N_{xy} due to the variable stiffness.

Representing the lamination parameters distribution in the form of B-splines (or NURBS) exhibits many advantages for the optimal design of VAT laminates. Usage of the B-splines allows the discretization scheme for the stiffness variation to be control-points based and independent of the modeling approach. In a finite element-based design approach [5], the design variables (lamination parameters) are associated with all elements (or nodes); therefore, the design flexibility is fixed to be the same as the degree of freedom of the finite element model. In addition, the number of design variables in a B-spline approach is much less than the finite element method. A smaller number of design variables not only simplifies the design process but also significantly reduces the computational cost for the sensitivities, which is the most time-consuming part in a gradient-based optimization process. Last, the finite element method requires

Table 1 First-level optimization results for the maximum buckling load K_x^{cr} of square VAT plates using different numbers of control points to construct the lamination parameter distribution[a]

	Case A		Case B	
Layups	K_{cr}^{*}	Increase, %	K_{cr}^{*}	Increase, %
QI	1	— —	1	— —
CS: ± 45 ($\xi_{1,2}^{D} = [0,-1]$)	1.29	— —	0.93	— —
CS: $[\pm 36/\mp 36/\pm 24/\mp 24/0_4]_{AS}$	— —	— —	1.27	— —
($\xi_{1,2}^{A,D} = [0.64, 0, 0.4, -0.6]$)	— —	— —		— —
VAT: 5×5	2.66	106.2	1.88	48.0
VAT: 7×7	2.89	124.0	1.96	54.3
VAT: 9×9	2.92	126.4	2.02	59.0
VAT: 11×11	2.92	126.4	2.04	60.6

[a]QI denotes quasi-isotropic laminate, and CS denotes constant-stiffness laminates.

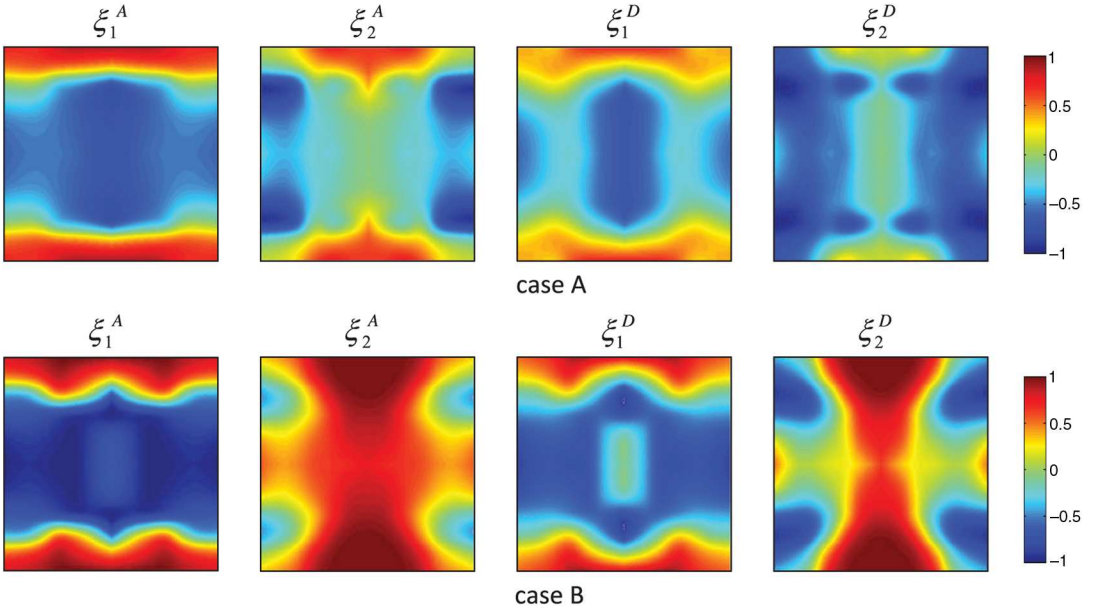

Fig. 6 Optimal lamination parameter distribution for a square VAT plate under two different in-plane boundary conditions (case A and case B): 7×7 control points.

additional constraints [5,14] for constructing a smooth lamination parameter variation; however, B-splines satisfy this requirement inherently.

2. *Long VAT Plates*

In this section, the design of infinitely long VAT plates for maximizing buckling performance is presented. The length of a VAT plate was selected to be 20 times its width ($a = 5.08$ m, $b = 0.254$ m) to adequately capture the (infinitely) long plate effect. Two different out-of-plane boundary conditions are studied: 1) four edges are all simply supported; and 2) one free edge and the rest are simply supported. As the majority of applied compressive load is redistributed toward the supported edges, the case of transversely varying lamination parameters is initially considered in the optimization. Thus, the four lamination parameters are varied along the y direction $\xi_{1,2}^{A,D}(y)$. For the simply supported boundary conditions, the stiffness variation is defined symmetrically with respect to the x axis, as

$$\xi_{1,2}^{A,D}(y) = \xi_{1,2}^{A,D}(|y|)$$

However, this symmetric condition is not valid in the design of the free-edge problem. For prismatic stiffness variation, closed-form solutions are available for computing the nonuniform in-plane stress [2,46]:

$$N_x = \left[A_{11}(y) - \frac{A_{12}^2(y)}{A_{22}(y)}\right]\frac{\Delta_x}{a} \tag{38}$$

Using Eq. (38) to model the prebuckling behavior of VAT plates can significantly reduce the computational cost of the buckling analysis and sensitivity evaluation. Figures 8 and 9 show the optimal

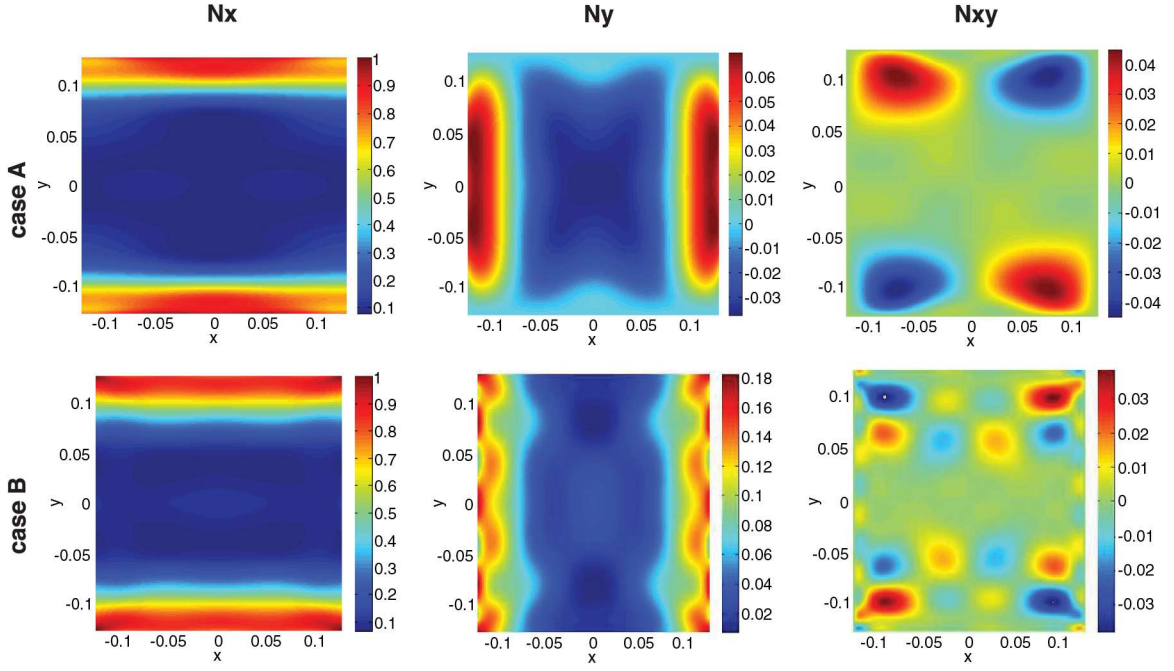

Fig. 7 In-plane stress distribution of VAT square plates with optimal lamination parameters (case A and case B).

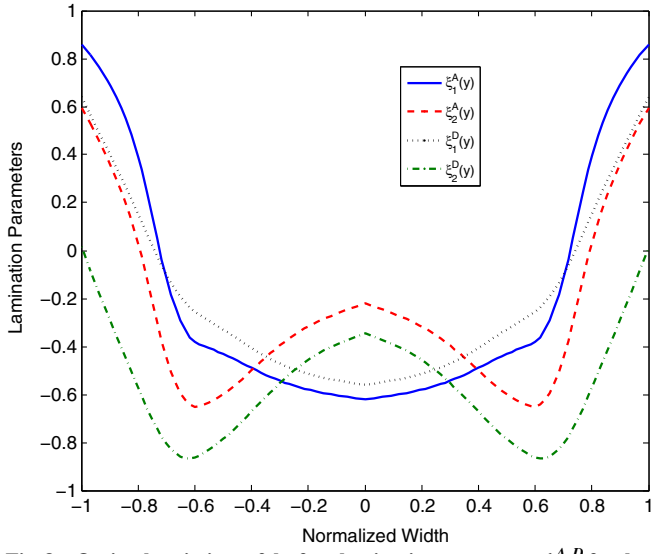

Fig. 8 Optimal variations of the four lamination parameters $\xi_{1,2}^{A,D}$ for the maximum buckling load of a VAT long plate (case A).

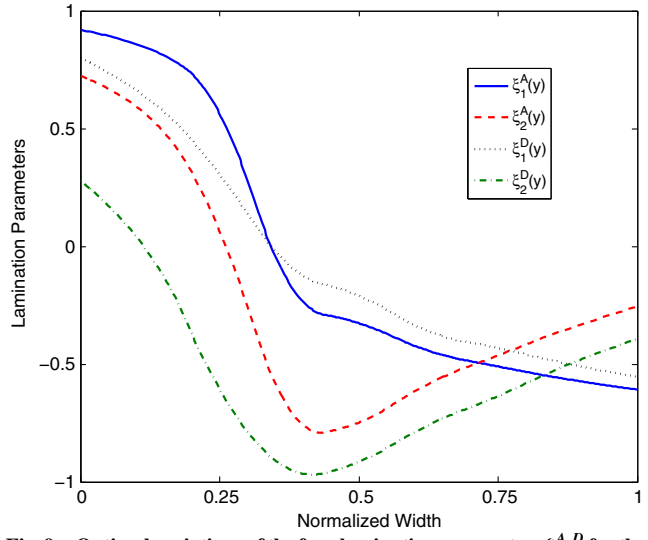

Fig. 9 Optimal variations of the four lamination parameters $\xi_{1,2}^{A,D}$ for the maximum buckling load of VAT plates with one free edge, and the others are simply supported.

variations of the four lamination parameters for the long VAT plates under both boundary conditions, in which seven (symmetric) and nine (unsymmetric) control points are used for achieving convergent results, respectively. For the case of simply supported boundary conditions, the maximum buckling coefficient is 2.61. For the free-edge problem, the maximum buckling coefficient is 4.12. Both of the results are slightly larger than the results obtained from a direct search using the genetic algorithm [3]. Nevertheless, no further improvement of buckling load was observed when the lamination parameters (stiffness) are allowed to vary along both axes for the long VAT plate.

B. Optimal VAT Layups (Second Level)

Realistic variation of fiber-orientation angles (or the tow trajectories) for the VAT lamination layups are now retrieved from the optimal lamination parameters obtained in the previous section. As previously mentioned, the stacking sequence is fixed to be a 16-layer unsymmetric, specially orthotropic laminate with two VAT design layers. In the optimization process, in each VAT design layer, the number of control points for defining the NLV of fiber-orientation angles [Eq. (32)] is gradually increased to obtain convergent results. In this section, the second-level optimization is carried out on the square plate (under case A) and the long VAT plate with one free edge.

Tables 2 and 3, respectively, present (for each problem) the optimal layups and the corresponding improvements of the buckling loads, which are obtained using two different optimization approaches. One is a direct GA search approach based on the definition of NLV of fiber-orientation angles to parameterize the VAT layups [3], and the other is the two-level optimization strategy presented herein. For a clear comparison, the number of control points along each direction that is used to define the NLV of fiber angles of VAT layups was selected to be the same for both methods. A 3×3 control-points grid is used in each VAT design layer for the square plate, and five control points along the y axis are used for the long plate with a free edge. The results presented in Tables 2 and 3 show that the determined optimal variation of fiber angles using these two methods are slightly different (in terms of the distribution), but they give nearly identical normalized buckling loads. This indicates that many optimal VAT layup configurations exist, which give similar buckling loads. This characteristic could benefit the design of VAT laminates when more (practical) constraints are introduced in the optimization process.

A direct GA search approach requires many (population size $\times$ the number of generations) buckling evaluation runs for the design of VAT plates. The computational effort increases considerably when many layers and control points are used. Nevertheless, this issue is avoided in the two-level optimization strategy. For these two problems, less than 10 iterations are required

Table 3 Optimal layups for the maximum buckling load of a long SSSF 16-layer specially orthotropic laminates

Methods	Layups	K_{cr}^*	Increase, %
— —	Quasi isotropic	1	— —
— —	$[\pm 45/\mp 45]_{AS}$	1.70	— —
Direct GA	$\theta_1 : T_{0.4} = [-11.5, 41.5, 56, 58, 65.5]$ $\theta_2 : T_{0.4} = [4, -20, -58, -67, -70]$	3.94	131.7
Two level	$\theta_1 : T_{0.4} = [17.5, 36.5, 52.5, 56, 64]$ $\theta_2 : T_{0.4} = [-5, -11, -51, -65, -68]$	3.95	132.3

Table 2 Optimal layups for the maximum buckling load of a square 16-layer specially orthotropic laminates (for case A)

Methods	Layups	K_{cr}^*	Increase, %
— —	Quasi isotropic	1	— —
— —	$[\pm 45/\mp 45]_{AS}$	1.29	— —
Direct GA	$\begin{bmatrix} 71 & 49.5 & 71.5 \\ 67 & 50 & 51 \\ 17 & 12 & 45 \end{bmatrix}^{\theta_1} \begin{bmatrix} -72.5 & -59 & -59.5 \\ -65 & -54 & -50.5 \\ 14 & 11.5 & 6 \end{bmatrix}^{\theta_2}$	2.71	110
Two level	$-\begin{bmatrix} 71.6 & 52.2 & 75.4 \\ 75 & 45.6 & 54.1 \\ 14.2 & 17.9 & 46.3 \end{bmatrix}^{\theta_1} \begin{bmatrix} 74 & 61.2 & 60.9 \\ 74.1 & 49.5 & 55.1 \\ -17.7 & -10.8 & -7.0 \end{bmatrix}^{\theta_2}$	2.73	112

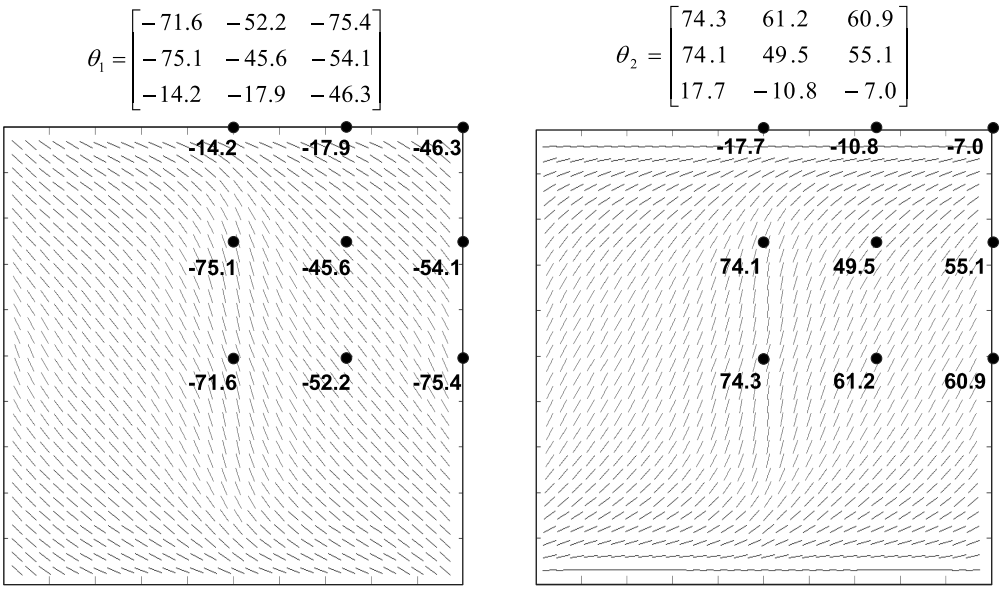

Fig. 10 The optimum nonlinear variation (3×3 control points for each layer) of fiber-orientation angles for maximum buckling load of the square simply supported VAT plate design for case A.

to achieve the optimal lamination parameter distribution for the theoretically possible maximum buckling load. The subsequent process of retrieving realistic layups from the resultant lamination parameters requires little computational effort, even when the design flexibility is extended.

Figures 10 and 11 show the spatially nonlinear varying fiber angle distributions of the optimal VAT layers for the maximum buckling load of the square VAT plate (case A) and the long VAT plate with a free edge, respectively. For the square plate, as shown in Fig. 10, most fiber angles in the domain are close to $45(-45)$ deg and the center region is filled with the $70 \sim 90$ deg fiber angles. The ± 45 deg plies are effective at suppressing buckling for the compressive-loaded square plate, whereas the overall variation of fiber angles in Fig. 10 contributes to the stress redistribution. In Fig. 11, for the design of a VAT plate with a free edge, the value of fiber angles of both layers are monotonically increasing from the bottom simply supported edge to the free edge. This variation of fiber angle gives rise to redistribution of the compression load toward the bottom (simply supported) edge. It is interesting to note that Figs. 10 and 11 show the fiber orientations are all approximately 0 deg near the supported transverse edges for the inner layers. The 0 deg fiber angles are useful for strengthening the plate, as the majority of the compressive load is redistributed to this region.

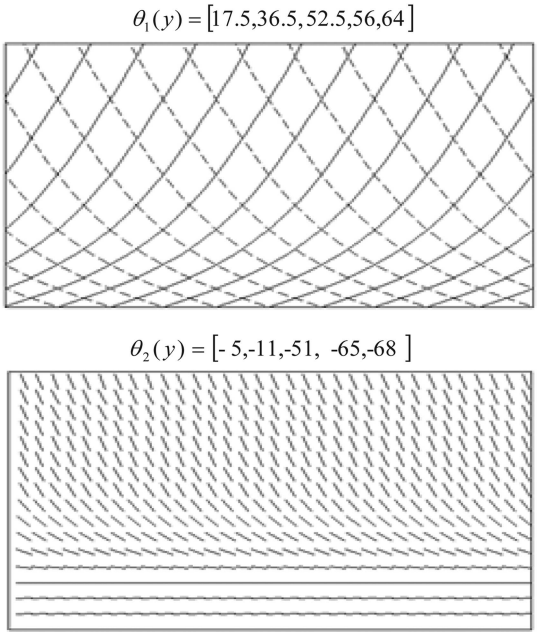

Fig. 11 Segment of the optimal NLV of fiber-orientation angles for the long VAT plate with a free edge: top shows $\theta_1(y)$, and bottom shows $\theta_2(y)$.

VI. Conclusions

A rapid design framework has been developed that combines efficient structural analysis (order-of-magnitude less design variables than finite element) with a computationally efficient two-level optimization strategy to perform the design of variable-angle tow composite plates for maximum buckling load. The structural analysis defines new expressions for structural stiffness, making for efficient and rapid analysis. Moreover, the newly derived 23 explicit nonlinear expressions for the four lamination parameters, which represent orthotropic laminates, also enables a more rapid optimization process for VAT laminates than previous works that use tens of thousands of linear constraints. The optimization strategy advances current methods for constant fiber-orientation laminates to allow the use of spatially varying lamination parameters to capture pointwise stiffness variation that are also guaranteed to be feasible pointwise, although only evaluated at a small number of discrete control points. This feature allows us to reduce the number of control points from one that is open ended to a small number, typically less than 10 along one direction.

Although finite element techniques either ignore spurious local stresses arising from the assumption of piecewise constant-stiffness properties or use additional smoothing steps, the current analysis inherently allows smooth distributions of both stiffness variation and fiber angles. The distributions of spatially varying lamination parameters and fiber angles are both characterized by different sets of predefined control points over the plate domain. The B-spline basis functions and Lagrangian polynomials are used to mathematically define the variations of lamination parameters and fiber angles, respectively. This control-points-based scheme is shown to require less design variables than a finite element approach and inherently results in smooth, continuous distributions. Furthermore, by using less grid points for the design of VAT plies from that used for the structural model leads to faster convergence in optimization studies than state-of-the-art methods that use the same finite element discretization schemes for both design and analysis.

Numerical examples on both square and long VAT plates under different boundary conditions and loading cases were conducted to show the computational efficiency and robustness of our approach. The optimal distributions of lamination parameters and the corresponding VAT laminate layups for the maximum buckling load match well with previous published results given by a direct GA search approach but with few control points, and therefore enhanced computational efficiency. In future work, this two-level design approach will be applied to optimize the postbuckling performance of VAT plates considering damage-tolerance requirements.

Appendix A: Feasible Region of Lamination Parameters

A1 Outer Boundary

The separate feasible region of in-plane or out-of-plane lamination parameters has been derived by Fukunaga and Sekine [18], and it expressed in the following form:

$$2(1+\xi_2^j)(\xi_3^j)^2 - 4\xi_1^j\xi_3^j\xi_4^j + (\xi_4^j)^2 - (\xi_2^j - 2(\xi_4^j)^2 + 1)(1-\xi_2^j) \le 0 \tag{A1}$$

$$(\xi_1^j)^2 + (\xi_3^j)^2 \le 1 \tag{A2}$$

where $j = A, D$. For the design problems that only involve pure in-plane or bending analyses (for example, the buckling of constant-stiffness symmetric laminates), the feasible region given by Eqs. (A1) and (A2) is sufficient to define the nonlinear constraints for lamination parameters. However, in cases that require a group of coupled lamination parameters, explicit expressions that can bound the feasible region accurately of lamination parameters are not available. Grenestedt and Gudmundson [19] provided a series of nonlinear inequalities by which an outer boundary of the feasible region can be obtained. The outer boundary may be sufficiently accurate and robust in some optimization problems for constant-stiffness composite laminates [35]. In the optimization of variable stiffness laminates, they do not provide sufficient constraints due to the continuous variation of the values of design variables. Therefore, Setoodeh et al. [20] and Ijsselmuiden et al. [5] used an approximate feasible region that was generated from a numerical approach using the method of convex hulls. The convex hull approach often results in a large number of linear inequalities to define an approximate bound for the feasible region, which may make subsequent optimization studies relatively unwieldy and inefficient.

In this section, the feasible region of two in-plane and two out-of-plane lamination parameters (ξ_1^A, ξ_2^A, ξ_1^D, ξ_2^D) for the design of orthotropic laminates is studied. The expressions for the in-plane and out-of-plane lamination parameters given by Eq. (A1) reduce to

$$2(\xi_1^A)^2 - 1 \le \xi_2^A \le 1 \tag{A3}$$

$$2(\xi_1^D)^2 - 1 \le \xi_2^D \le 1 \tag{A4}$$

Both Eqs. (A3) and (A4) form the parabolic relation for each set of lamination parameters. Grenestedt and Gudmundson [19] derived the following explicit expressions that could link these lamination parameters:

$$\frac{1}{4}(\xi_1^A+1)^3 - 1 \le \xi_1^D \le \frac{1}{4}(\xi_1^A-1)^3 + 1 \tag{A5}$$

$$\frac{1}{4}(\xi_2^A+1)^3 - 1 \le \xi_2^D \le \frac{1}{4}(\xi_2^A-1)^3 + 1 \tag{A6}$$

Equations (A5) and (A6) are necessary conditions derived from a variational method, but they are far from the sufficient conditions that define the boundary of the feasible region accurately. The Schwarz inequality was applied to derive further connections for the coupled lamination parameters [19]:

$$\int f^2 \,\mathrm{d}\bar{z} \int g^2 \,\mathrm{d}\bar{z} - \left(\int fg \,\mathrm{d}\bar{z}\right)^2 \ge 0 \tag{A7}$$

In Eq. (A7), $f = \bar{z}^2 + e$ and $g = \cos(2\theta)$ are chosen to derive the relations for the lamination parameters $\xi_{1,2}^A$, ξ_2^D. The following inequality is obtained when the left side of Eq. (A7) is minimized with respect to the variable e:

$$5(\xi_1^A - \xi_1^D)^2 - 2(1 + \xi_2^A - 2(\xi_1^A)^2) \le 0 \tag{A8}$$

Applying different expressions of f and g to Eq. (A7) can achieve more constraints, which can build up the connections between the lamination parameters of ξ_i^A, ξ_i^B, and ξ_i^D (see appendix A.2 of [19]). We examined these derived constraints for the four lamination parameters $\xi_{1,2}^{A,D}$ (others are zero), noting that only the conditions given by Eqs. (A3–A6) and (A8) were found to be active.

Finally, Eqs. (A3–A6) and (5) give an outer boundary of the feasible region, which is appropriate for the optimization of the constant-stiffness laminates [35,36]. Nevertheless, for the optimization problem of VAT composite laminates, such an outer boundary was found in this work to not be sufficiently accurate, and it needs further refinement.

A2 New Constraints

A more accurate boundary for the feasible region can be derived based on Bloomfield et al.'s work [21], in which stronger links between the lamination parameters from each design subspace are obtained by using the following algebraic identity [12]:

$$4(z_x - z_y)(z_x^3 - z_y^3) = (z_x - z_y)^4 + 3(z_x^2 - z_y^2)^2 \tag{A9}$$

where z_x or z_y indicate the distance of a ply to the midplane. On the boundary of the feasible region, it was proved that

$$\begin{cases} z_x - z_y = \frac{1}{k}(h_1\xi_1^A + h_2\xi_2^A + h_3\xi_3^A + h_4\xi_4^A + h_5) \\ z_x^2 - z_y^2 = \frac{1}{k}(h_1\xi_1^B + h_2\xi_2^B + h_3\xi_3^B + h_4\xi_4^B + h_5) \\ z_x^3 - z_y^3 = \frac{1}{k}(h_1\xi_1^D + h_2\xi_2^D + h_3\xi_3^D + h_4\xi_4^D + h_5) \end{cases} \tag{A10}$$

where each vector $\boldsymbol{h} = \{h_1, h_2, h_3, h_4, h_5\}^T$ denotes a hyperplane constraint along the boundary of the feasible regions for the in-plane, coupling, and out-of-plane lamination parameters. Here, the k is a scaling factor given by [21]

$$k = \max\left(\frac{1}{2}\sum_i^5 h_i\xi_i^A\right); \qquad (\xi_5^A = 1) \tag{A11}$$

The following two expressions that connect the in-plane, coupling, and out-of-plane hyperplane constraints were obtained by Bloomfield et al. [21]:

$$\begin{aligned} &4k^2\left(\sum_{i=1}^4 h_i\xi_i^A - H^L\right)\left(\sum_{i=1}^4 h_i\xi_i^D - H^L\right) \\ &\ge \left(\sum_{i=1}^4 h_i\xi_i^A - H^L\right)^4 + 3k^2\left(\sum_{i=1}^4 h_i\xi_i^B\right)^2 \end{aligned} \tag{A12}$$

$$4k^2\left(\sum_{i=1}^{4} h_i\xi_i^A - H^U\right)\left(\sum_{i=1}^{4} h_i\xi_i^D - H^U\right) \geq \left(\sum_{i=1}^{4} h_i\xi_i^A - H^U\right)^4 + 3k^2\left(\sum_{i=1}^{4} h_i\xi_i^B\right)^2 \tag{A13}$$

where H^L and H^U are the lower and upper bounds of each hyperplane constraint, respectively. It was proved that Eqs. (A12) and (A13) establish strong links between the in-plane, coupling, and out-of-plane lamination parameters for any predefined, finite set of fiber orientation. For example, Bloomfield et al. [21] presented explicit expressions for the boundary of the feasible region of the 12 lamination parameters, which are for ply angles fixed in the finite set of 0, 90, ±30, ±45, ±60.

To derive explicit formulas for the general feasible region of lamination parameters, the set of fiber orientations is assumed to enclose an infinite number of discretized ply angles ($-90 \leq \theta_i \leq 90$, $i = 1, 2, \cdots, \infty$). Equations (A12) and (A13) remain to be validated with the given hyperplanes, but they represent an infinite number of expressions. In this case, each hyperplane $\boldsymbol{h} = \{h_1, h_2, h_3, h_4, h_5\}^T$ in Eqs. (A12) and (A13) is, or is parallel to, a particular tangent plane to the boundary surface of the feasible region at the point of $(\xi_i^{A,B,D})$.

As only four lamination parameters of ξ_1^A, ξ_2^A, ξ_1^D, and ξ_2^D are required (for orthotropic laminates), Eqs. (A12) and (A13) reduce to

$$(h_1\xi_1^A + h_2\xi_2^A - H^L)^4 - 4k^2(h_1\xi_1^A + h_2\xi_2^A - H^L)(h_1\xi_1^D + h_2\xi_2^D - H^L) \leq 0 \tag{A14}$$

$$(h_1\xi_1^A + h_2\xi_2^A - H^U)^4 - 4k^2(h_1\xi_1^A + h_2\xi_2^A - H^U)(h_1\xi_1^A + h_2\xi_2^A - H^U) \leq 0 \tag{A15}$$

Both the feasible regions of (ξ_1^A, ξ_2^A) and (ξ_1^D, ξ_2^D) form parabolas. Therefore, the direction of each hyperplane in Eqs. (A14) and (A15) corresponds to a tangent line of the parabola defined in Eq. (A3) or (A4). The parabola is written in general form as $s = 2t^2 - 1$ ($t \in [-1, 1]$), and the vector $\{h_1, h_2\}^T$ for the hyperplane has the following closed-form expression in terms of t:

$$h_1 = \frac{4t}{1+2t^2}, \qquad h_2 = -\frac{1}{1+2t^2} \tag{A16}$$

Subsequently, H^L, H^U can be determined in closed form by obtaining the minimum and maximum values of the following function:

$$f(\xi_1^{A,D}, \xi_2^{A,D}) = h_1\xi_1^{A,D} + h_2\xi_2^{A,D} \Rightarrow$$
$$f(\xi_1^{A,D}) = \frac{4t}{1+2t^2}\xi_1^{A,D} - \frac{1}{1+2t^2}(2(\xi_1^{A,D})^2 - 1) \Rightarrow$$
$$H^U = 1, \qquad H^L = -\frac{4|t|+1}{1+2t^2} \tag{A17}$$

Figure A1 illustrates the geometric relations between the parabolic feasible region and the deduced hyperplanes, as well as the upper and lower limits (H^U, H^L). It can be observed that this parabolic feasible region is discretized into infinite sets of hyperplanes; fortunately, these hyperplanes can be defined generally by closed-form expressions [Eqs. (A16) and (A17)]. Substituting the expressions of h_1, h_2, H^L, and H^U into Eq. (A11), the scaling factor k is determined as

$$k^2 = \left(\frac{-|h_1| + h_2 - 1}{2}\right)^2 = \left(\frac{1+2|t|+t^2}{1+2t^2}\right)^2 \tag{A18}$$

Substituting Eqs. (A16–A18) into Eqs. (A14) and (A15), explicit expressions are obtained and written as

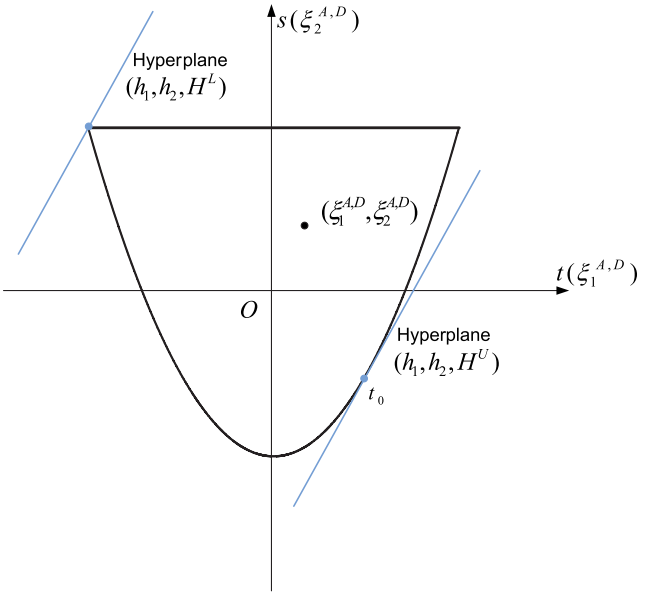

Fig. A1 Geometric illustration of the hyperplanes along the boundary of a parabolic feasible region.

$$(4t\xi_1^A - \xi_2^A - 1 - 2t^2)^4 - 4(1+2|t|+t^2)^2(4t\xi_1^A - \xi_2^A - 1 - 2t^2)(4t\xi_1^D - \xi_2^D - 1 - 2t^2) \leq 0 \tag{A19}$$

$$(4t\xi_1^A - \xi_2^A + 1 + 4|t|)^4 - 4(1+2|t|+t^2)^2(4t\xi_1^A - \xi_2^A + 1 + 4|t|)(4t\xi_1^D - \xi_2^D + 1 + 4|t|) \leq 0 \tag{A20}$$

Due to parabolic constraints the in Eqs. (A3) and (A4), the following relations are derived:

$$\xi_2^A - 4t\xi_1^A + 1 + 2t^2 \geq 2(\xi_1^A)^2 - 4t\xi_1^A + 2t^2 = 2(\xi_1^A - t)^2 \geq 0$$
$$4t\xi_1^A - \xi_2^A + 1 + 4|t| = 4|t|(1 \pm \xi_1^A) + (1 - \xi_2^A) \geq 0 \tag{A21}$$

Equations (A19) and (A20) are further simplified to

$$(\xi_2^A - 4t\xi_1^A + 1 + 2t^2)^3 - 4(1+2|t|+t^2)^2(\xi_2^D - 4t\xi_1^D + 1 + 2t^2) \leq 0 \tag{A22}$$

$$(4t\xi_1^A - \xi_2^A + 1 + 4|t|)^3 - 4(1+2|t|+t^2)^2(4t\xi_1^D - \xi_2^D + 1 + 4|t|) \leq 0 \tag{A23}$$

In principle, the lamination parameters ξ_1^A, ξ_2^A, ξ_1^D, and ξ_2^D have to satisfy the constraints given by Eqs. (A22) and (A23) for all $t \in [-1, 1]$ or, alternatively, t is determined analytically in closed form by maximizing the left sides of Eqs. (A22) and (A23). Nevertheless, it was found that a set of nonlinear inequalities generated from Eqs. (A22) and (A23) with only a few discretized points of t are also capable of representing the boundary of the feasible region of the four lamination parameters $(\xi_1^A, \xi_2^A, \xi_1^D, \xi_2^D)$ with good accuracy. It was found by trial and error that a value of t between

$$[-1, -0.75, -0.5, -0.25, 0, 0.25, 0.5, 0.75, 1]$$

was found to be sufficiently accurate or, for better accuracy,

$$t = [-1, -0.8, -0.6, -0.4, -0.2, 0, 0.2, 0.4, 0.6, 0.8, 1]$$

It was found that the set of equations in Eqs. (A8–A23) are able to bound the entire feasible region of the four lamination parameters ($\xi_{1,2}^{A,D}$) with sufficiently good accuracy. Now, all the constraints that were obtained for defining the feasible region of these four lamination parameters ξ_1^A, ξ_2^A, ξ_1^D, and ξ_2^D are Eqs. (A3–A6), (A8), (A22), and (A23). In fact, Eqs. (A8), (A22), and (A23) provide strong constraints for these lamination parameters, and they implicitly contain the relations defined by Eqs. (A3–A6). For example, from Eq. (A8), it can be deduced that

$$\begin{aligned}&5(\xi_1^A-\xi_1^D)^2-2(1+\xi_2^A-2(\xi_1^A)^2)\le 0\Rightarrow\\&2(1+\xi_2^A-2(\xi_1^A)^2)\ge 5(\xi_1^A-\xi_1^D)^2\ge 0\Rightarrow\\&2(\xi_1^A)^2-1\le\xi_2^A\end{aligned}\tag{A24}$$

Equations (A22) and (A23) also reduce to Eq. (A6) when t is equal to zero. Finally, it was shown that Eqs. (A8), (A22), and (A23) are sufficient to generate a relatively accurate boundary for the feasible region of $\xi_{1,2}^{A,D}$ in which only $19\sim 23$ nonlinear inequalities are required. Hence, this approach requires much less computational effort in an optimization process than the convex hull approach [17], which employs 37,126 linear equations to approximately bound the feasible region, and which was implemented in the optimization framework developed recently developed by Ijsselmuiden et al. [5] and Nagy et al. [25].

Figure A2 demonstrates the intersections of the feasible region with different planes, in which the solid lines represent the feasible region defined by the explicit formulas; the dashed lines indicate the true feasible region generated using a numerical procedure [12] and the outer boundary derived by Grenestedt and Gudmundson [19] is indicated by the dashed–dotted lines. Good agreement of the intersections between the results given by the explicit formulas and the numerical solution is shown in Fig. A2. The outer boundary of the feasible region given by Grenestedt and Gudmundson [19] is also shown in Fig. A2 as the dashed–dotted lines, which clearly demonstrate the contribution of the newly derived constraints [Eqs. (A22) and (A23)] to the boundary of the feasible region.

Appendix B: Expressions for Buckling Analysis

The explicit forms for the stiffness tensors in the buckling model [Eqs. (22) and (23)] are expressed in the following. The aspect ratio of VAT plates (a/b) is denoted by R. Each element in matrices K_0^b, K_1^b, and K_2^b is given by

$$\begin{aligned}K^b_{0(mn\bar{m}\,\bar{n})}=&\frac{h^3}{12}\int_{-1}^{1}\int_{-1}^{1}[U_1X^w_{m,\xi\xi}Y^w_nX^w_{\bar{m},\xi\xi}Y^w_{\bar{n}}\\&+R^2U_4(X^w_mY^w_{n,\eta\eta}X^w_{\bar{m},\xi\xi}Y^w_{\bar{n}}+X^w_{m,\xi\xi}Y^w_nX^w_{\bar{m}}Y^w_{\bar{n},\eta\eta})\\&+R^4U_1X^w_mY^w_{n,\eta\eta}X^w_{\bar{m}}Y^w_{\bar{n},\eta\eta}+4R^2U_5X^w_{m,\xi}Y^w_{n,\eta}X^w_{\bar{m},\xi}Y^w_{\bar{n},\eta}]\mathrm{d}\xi\,\mathrm{d}\eta\end{aligned}\tag{B1}$$

$$\begin{aligned}K^b_{1(mn\bar{m}\,\bar{n})}=&\frac{h^3}{12}U_2\int_{t_r}^{t_{r+k}}\int_{t_s}^{t_{s+k}}[N^{(k)}_rN^{(k)}_s\tilde{X}^w_{m,\xi\xi}\tilde{Y}^w_n\tilde{X}^w_{\bar{m},\xi\xi}\tilde{Y}^w_{\bar{n}}\\&-R^4N^{(k)}_rN^{(k)}_s\tilde{X}^w_m\tilde{Y}^w_{n,\eta\eta}\tilde{X}^w_{\bar{m}}\tilde{Y}^w_{\bar{n},\eta\eta}]\mathrm{d}\bar{u}\,\mathrm{d}\bar{v}\end{aligned}\tag{B2}$$

$$\begin{aligned}K^b_{2(mn\bar{m}\,\bar{n})}=&\frac{h^3}{12}U_3\int_{t_r}^{t_{r+k}}\int_{t_s}^{t_{s+k}}[N^{(k)}_rN^{(k)}_s\tilde{X}^w_{m,\xi\xi}\tilde{Y}^w_n\tilde{X}^w_{\bar{m},\xi\xi}\tilde{Y}^w_{\bar{n}}\\&+R^4N^{(k)}_rN^{(k)}_s\tilde{X}^w_m\tilde{Y}^w_{n,\eta\eta}\tilde{X}^w_{\bar{m}}\tilde{Y}^w_{\bar{n},\eta\eta}-\\&R^2(N^{(k)}_rN^{(k)}_s\tilde{X}^w_m\tilde{Y}^w_{n,\eta\eta}\tilde{X}^w_{\bar{m},\xi\xi}\tilde{Y}^w_{\bar{n}}+N^{(k)}_rN^{(k)}_s\tilde{X}^w_{m,\xi\xi}\tilde{Y}^w_n\tilde{X}^w_{\bar{m}}\tilde{Y}^w_{\bar{n},\eta\eta})\\&-4R^2N^{(k)}_rN^{(k)}_s\tilde{X}^w_{m,\xi}\tilde{Y}^w_{n,\eta}\tilde{X}^w_{\bar{m},\xi}\tilde{Y}^w_{\bar{n},\eta}]\mathrm{d}\bar{u}\,\mathrm{d}\bar{v}\end{aligned}\tag{B3}$$

The expression for each element in the matrices of $K^s_{10}, K^s_{11}, \cdots, K^s_{22}$ is

$$\begin{aligned}K^s_{10(mn\bar{m}\,\bar{n})}=&h\int_{-1}^{1}\int_{-1}^{1}[U_1X^u_{p,\xi}Y^u_qX^w_{m,\xi}Y^w_nX^w_{\bar{m},\xi}Y^w_{\bar{n}}\\&+R^2U_4X^u_{p,\xi}Y^u_qX^w_mY^w_{n,\eta}X^w_{\bar{m}}Y^w_{\bar{n},\eta}\\&+R^2U_5(X^u_pY^u_{q,\eta}X^w_{m,\xi}Y^w_nX^w_{\bar{m}}Y^w_{\bar{n},\eta}+X^u_pY^u_{q,\eta}X^w_mY^w_{n,\eta}X^w_{\bar{m},\xi}Y^w_{\bar{n}})]\mathrm{d}\xi\,\mathrm{d}\eta\end{aligned}\tag{B4}$$

$$K^s_{11(mn\bar{m}\,\bar{n})}=hU_2\int_{t_r}^{t_{r+k}}\int_{t_s}^{t_{s+k}}N^{(k)}_rN^{(k)}_s\tilde{X}^u_{p,\xi}\tilde{Y}^u_q\tilde{X}^w_{m,\xi}\tilde{Y}^w_n\tilde{X}^w_{\bar{m},\xi}\tilde{Y}^w_{\bar{n}}\,\mathrm{d}\bar{u}\,\mathrm{d}\bar{v}\tag{B5}$$

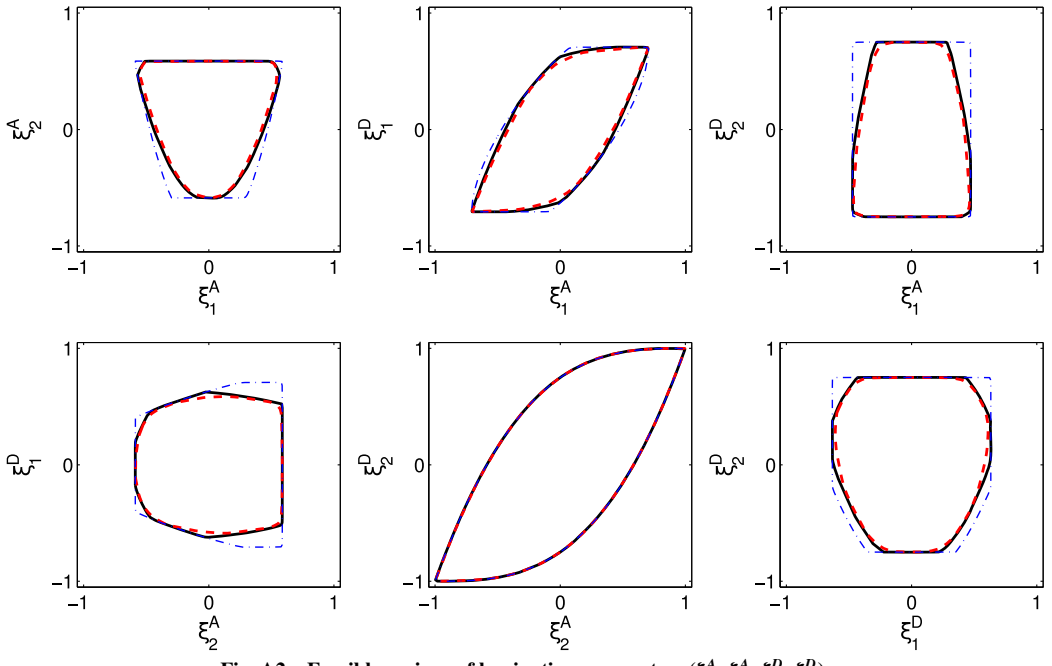

Fig. A2 Feasible regions of lamination parameters (ξ_1^A, ξ_2^A, ξ_1^D, ξ_2^D).

$$K^s_{12(mn\bar{m}\,\bar{n})} = hU_3 \int_{t_r}^{t_{r+k}} \int_{t_s}^{t_{s+k}} [N_r^{(k)} N_s^{(k)} \tilde{X}^u_{p,\xi} \tilde{Y}^u_q \tilde{X}^w_{m,\xi} \tilde{Y}^w_n \tilde{X}^w_{\bar{m},\xi} \tilde{Y}^w_{\bar{n}}$$
$$- R^2 N_r^{(k)} N_s^{(k)} \tilde{X}^u_{p,\xi} \tilde{Y}^u_q \tilde{X}^w_m \tilde{Y}^w_{n,\eta} \tilde{X}^w_{\bar{m}} \tilde{Y}^w_{\bar{n},\eta}$$
$$- R^2 (N_r^{(k)} N_s^{(k)} \tilde{X}^u_p \tilde{Y}^u_{q,\eta} \tilde{X}^w_{m,\xi} \tilde{Y}^w_n \tilde{X}^w_{\bar{m}} \tilde{Y}^w_{\bar{n},\eta}$$
$$+ N_r^{(k)} N_s^{(k)} \tilde{X}^u_p \tilde{Y}^u_{q,\eta} \tilde{X}^w_m \tilde{Y}^w_{n,\eta} \tilde{X}^w_{\bar{m},\xi} \tilde{Y}^w_{\bar{n}})]\,\mathrm{d}\bar{u}\,\mathrm{d}\bar{v} \tag{B6}$$

$$K^s_{20(mn\bar{m}\,\bar{n})} = h \int_{-1}^{1} \int_{-1}^{1} [RU_4 X^v_p Y^v_{q,\eta} X^w_{m,\xi} Y^w_n X^w_{\bar{m},\xi} Y^w_{\bar{n}}$$
$$+ R^3 U_1 X^v_p Y^v_{q,\eta} X^w_m Y^w_{n,\eta} X^w_{\bar{m}} Y^w_{\bar{n},\eta}$$
$$+ R^2 U_5 (X^v_{p,\eta} Y^v_q X^w_{m,\xi} Y^w_n X^w_{\bar{m}} Y^w_{\bar{n},\eta}$$
$$+ X^v_{p,\eta} Y^v_q X^w_m Y^w_{n,\eta} X^w_{\bar{m},\xi} Y^w_{\bar{n}})]\mathrm{d}\xi\,\mathrm{d}\eta \tag{B7}$$

$$K^s_{21(mn\bar{m}\,\bar{n})} = hR^3 U_2 \int_{t_r}^{t_{r+k}} \int_{t_s}^{t_{s+k}} N_r^{(k)} N_s^{(k)} \tilde{X}^v_p \tilde{Y}^v_{q,\eta} \tilde{X}^w_m \tilde{Y}^w_{n,\eta} \tilde{X}^w_{\bar{m}} \tilde{Y}^w_{\bar{n},\eta} \mathrm{d}\bar{u}\mathrm{d}\bar{v} \tag{B8}$$

$$K^s_{22(mn\bar{m}\,\bar{n})} = hRU_3 \int_{t_r}^{t_{r+k}} \int_{t_s}^{t_{s+k}} [R^2 N_r^{(k)} N_s^{(k)} \tilde{X}^v_p \tilde{Y}^v_{q,\eta} \tilde{X}^w_m \tilde{Y}^w_{n,\eta} \tilde{X}^w_{\bar{m}} \tilde{Y}^w_{\bar{n},\eta}$$
$$- N_r^{(k)} N_s^{(k)} \tilde{X}^v_p \tilde{Y}^v_{q,\eta} \tilde{X}^w_{m,\xi} \tilde{Y}^w_n \tilde{X}^w_{\bar{m},\xi} \tilde{Y}^w_{\bar{n},\eta}$$
$$- (N_r^{(k)} N_s^{(k)} \tilde{X}^v_{p,\xi} \tilde{Y}^v_q \tilde{X}^w_{m,\xi} \tilde{Y}^w_n \tilde{X}^w_{\bar{m}} \tilde{Y}^w_{\bar{n},\eta}$$
$$+ N_r^{(k)} N_s^{(k)} \tilde{X}^v_{p,\xi} \tilde{Y}^v_q \tilde{X}^w_m \tilde{Y}^w_{n,\eta} \tilde{X}^w_{\bar{m},\xi} \tilde{Y}^w_{\bar{n}})]\mathrm{d}\bar{u}\,\mathrm{d}\bar{v} \tag{B9}$$

where $m, \bar{m} = 1, 2, \cdots, M$ and $n, \bar{n} = 1, 2, \cdots, N$.

The in-plane stiffness matrix K^m in the prebuckling model [Eq. (10)] consists of four submatrices that are

$$K^m = \begin{bmatrix} K^u & K^{uv} \\ (K^{uv})^T & K^v \end{bmatrix} \tag{B10}$$

Each matrix in Eq. (B10) is also expanded in terms of lamination parameters and rewritten in the following form:

$$K^\chi = K^\chi_0 + \sum_{rs} \Gamma^{(1)}_{rs} K^\chi_1 + \sum_{rs} \Gamma^{(2)}_{rs} K^\chi_2 \tag{B11}$$

where $\chi = \boldsymbol{u}, \boldsymbol{uv}, \boldsymbol{v}$ indicates different submatrices of Eq. (B10). The explicit expressions of these matrices for the prebuckling model are

$$K^u_{0(pq\bar{p}\,\bar{q})} = h \int_{-1}^{1} \int_{-1}^{1} [U_1 X^u_{p,\xi} Y^u_q X^u_{\bar{p},\xi} Y^u_{\bar{q}}$$
$$+ R^2 U_5 X^u_p Y^u_{q,\eta} X^u_{\bar{p}} Y^u_{\bar{q},\eta}]\mathrm{d}\xi\,\mathrm{d}\eta \tag{B12}$$

$$K^u_{1(pq\bar{p}\,\bar{q})} = hU_2 \int_{t_r}^{t_{r+k}} \int_{t_s}^{t_{s+k}} N_r^{(k)} N_{r,s} \tilde{X}^u_{p,\xi} \tilde{Y}^u_q \tilde{X}^u_{\bar{p},\xi} \tilde{Y}^u_{\bar{q}}\,\mathrm{d}\bar{u}\,\mathrm{d}\bar{v} \tag{B13}$$

$$K^u_{2(pq\bar{p}\,\bar{q})} = h \int_{t_r}^{t_{r+k}} \int_{t_s}^{t_{s+k}} [U_3 N_r^{(k)} N_{r,s} \tilde{X}^u_{p,\xi} \tilde{Y}^u_q \tilde{X}^u_{\bar{p},\xi} \tilde{Y}^u_{\bar{q}}$$
$$- R^2 U_5 N_r^{(k)} N_{r,s} \tilde{X}^u_p \tilde{Y}^u_{q,\eta} \tilde{X}^u_{\bar{p}} \tilde{Y}^u_{\bar{q},\eta}]\,\mathrm{d}\bar{u}\,\mathrm{d}\bar{v} \tag{B14}$$

$$K^{uv}_{0(pq\bar{p}\,\bar{q})} = hR \int_{-1}^{1} \int_{-1}^{1} [U_4 X^v_p Y^v_{q,\eta} X^u_{\bar{p},\xi} Y^u_{\bar{q}} + U_5 X^v_{p,\xi} Y^v_q X^u_{\bar{p}} Y^u_{\bar{q},\eta}]\mathrm{d}\xi\,\mathrm{d}\eta \tag{B15}$$

$$K^{uv}_{1(pq\bar{p}\,\bar{q})} = 0 \tag{B16}$$

$$K^{uv}_{2(pq\bar{p}\,\bar{q})} = -hR \int_{t_r}^{t_{r+k}} \int_{t_s}^{t_{s+k}} [U_3 N_r^{(k)} N_{r,s} \tilde{X}^v_p \tilde{Y}^v_{q,\eta} \tilde{X}^u_{\bar{p},\xi} \tilde{Y}^u_{\bar{q}}$$
$$+ U_5 N_r^{(k)} N_{r,s} \tilde{X}^v_{p,\xi} \tilde{Y}^v_q \tilde{X}^u_{\bar{p}} \tilde{Y}^u_{\bar{q},\eta}]\mathrm{d}\bar{u}\,\mathrm{d}\bar{v} \tag{B17}$$

$$K^v_{0(pq\bar{p}\,\bar{q})} = h \int_{-1}^{1} \int_{-1}^{1} [R^2 U_1 X^v_p Y^v_{q,\eta} X^v_{\bar{p}} Y^v_{\bar{q},\eta}$$
$$+ U_5 X^v_{p,\xi} Y^v_q X^u_{\bar{p},\xi} Y^v_{\bar{q}}]\mathrm{d}\xi\,\mathrm{d}\eta \tag{B18}$$

$$K^v_{1(pq\bar{p}\,\bar{q})} = -hU_3 \int_{t_r}^{t_{r+k}} \int_{t_s}^{t_{s+k}} N_r^{(k)} N_{r,s} \tilde{X}^v_p \tilde{Y}^v_{q,\eta} \tilde{X}^v_{\bar{p}} \tilde{Y}^v_{\bar{q},\eta} \mathrm{d}\bar{u}\mathrm{d}\bar{v} \tag{B19}$$

$$K^v_{2(pq\bar{p}\,\bar{q})} = h \int_{t_r}^{t_{r+k}} \int_{t_s}^{t_{s+k}} [R^2 U_3 N_r^{(k)} N_{r,s} \tilde{X}^v_p \tilde{Y}^v_{q,\eta} \tilde{X}^v_{\bar{p}} \tilde{Y}^v_{\bar{q},\eta}$$
$$- U_5 N_r^{(k)} N_{r,s} \tilde{X}^v_{p,\xi} \tilde{Y}^v_q \tilde{X}^v_{\bar{p},\xi} \tilde{Y}^v_{\bar{q}}]\mathrm{d}\bar{u}\,\mathrm{d}\bar{v} \tag{B20}$$

where $p, \bar{p} = 1, 2, \cdots, P_1(P_2)$ and $q, \bar{q} = 1, 2, \cdots, Q_1(Q_2)$.

Acknowledgments

The authors wish to acknowledge the Engineering and Physical Sciences Research Council, The Airbus Company, and GKN, plc., for supporting this research under the project Airbus, Bristol, Bath STrategic Research Alliance in Composites Technology (EP/H026371/1).

References

[1] Olmedo, R., and Gürdal, Z., "Buckling Response of Laminates with Spatially Varying Fiber Orientations," *34th AIAA/ASME/ASCE Structures, Structural Dynamics & Materials Conference*, AIAA, Washington, D.C., April 1993, pp. 2261–2269.

[2] Gürdal, Z., Tatting, B., and Wu, C., "Variable Stiffness Composite Panels: Effects of Stiffness Variation on the In-Plane and Buckling Response," *Composites, Part A: Applied Science and Manufacturing*, Vol. 39, No. 5, 2008, pp. 911–922. doi:10.1016/j.compositesa.2007.11.015

[3] Wu, Z., Weaver, P. M., Raju, G., and Kim, B. C., "Buckling Analysis and Optimisation of Variable Angle Tow Composite Plates," *Thin-Walled Structures*, Vol. 60, Nov. 2012, pp. 163–172. doi:10.1016/j.tws.2012.07.008

[4] Wu, Z., Weaver, P. M., and Raju, G., "Postbuckling Optimisation of Variable Angle Tow Composite Plates," *Composite Structures*, Vol. 103, Sept. 2013, pp. 34–42. doi:10.1016/j.compstruct.2013.03.004

[5] Ijsselmuiden, S. T., Abdalla, M. M., and Gürdal, Z., "Optimization of Variable-Stiffness Panels for Maximum Buckling Load Using Lamination Parameters," *AIAA Journal*, Vol. 48, No. 1, 2010, pp. 134–143. doi:10.2514/1.42490

[6] Ghiasi, H., Fayazbakhsh, K., Pasini, D., and Lessard, L., "Optimum Stacking Sequence Design of Composite Materials Part II: Variable Stiffness Design," *Composite Structures*, Vol. 93, No. 1, 2010, pp. 1–13. doi:10.1016/j.compstruct.2010.06.001

[7] Setoodeh, S., Abdalla, M. M., Ijsselmuiden, S. T., and Gürdal, Z., "Design of Variable-Stiffness Composite Panels for Maximum Buckling Load," *Composite Structures*, Vol. 87, No. 1, 2009, pp. 109–117. doi:10.1016/j.compstruct.2008.01.008

[8] Van Campen, J. M., Kassapoglou, C., and Gürdal, Z., "Generating Realistic Laminate Fiber Angle Distributions for Optimal Variable Stiffness Laminates," *Composites, Part B: Engineering*, Vol. 43, No. 2, 2012, pp. 354–360. doi:10.1016/j.compositesb.2011.10.014

[9] Tsai, S. W., Halpin, J. C., and Pagano, N. J., "Invariant Properties of Composite Materials," *Composite Materials Workshop*, Technomic Publ., Westport, CT, 1968, pp. 223–253.

[10] Miki, M., and Sugiyama, Y., "Optimum Design of Laminated, Composite Plates Using Lamination Parameters," *AIAA Journal*, Vol. 31, No. 5, 1993, pp. 921–922. doi:10.2514/3.49033

[11] Fukunaga, H., Sekine, H., Sato, M., and Iino, A., "Buckling Design of Symmetrically Laminated Plates Using Lamination Parameters," *Computers and Structures*, Vol. 57, No. 4, 1995, pp. 643–649. doi:10.1016/0045-7949(95)00050-Q

[12] Diaconu, C. G., Sato, M., and Sekine, H., "Feasible Region in General Design Space of Lamination Parameters for Laminated Composites," *AIAA Journal*, Vol. 40, No. 3, 2002, pp. 559–565. doi:10.2514/2.1683

[13] Setoodeh, S., Abdalla, M. M., and Gürdal, Z., "Design of Variable Stiffness Laminates Using Lamination Parameters," *Composites Part B: Engineering*, Vol. 37, Nos. 4–5, 2006, pp. 301–309. doi:10.1016/j.compositesb.2005.12.001

[14] Abdalla, M. M., Setoodeh, S., and Gürdal, Z., "Design of Variable Stiffness Composite Panels for Maximum Fundamental Frequency Using Lamination Parameters," *Composite Structures*, Vol. 81, No. 2, 2007, pp. 283–291. doi:10.1016/j.compstruct.2006.08.018

[15] Ijsselmuiden, S. T., "Optimal Design of Variable Stiffness Composite Structures Using Lamination Parameters," Ph.D. Thesis, Delft Univ. of Technology, Deft, The Netherlands, 2011.

[16] Svanberg, K., "A Class of Globally Convergent Optimization Methods Based on Conservative Convex Separable Approximations," *SIAM Journal on Optimization*, Vol. 12, No. 2, 2002, pp. 555–573. doi:10.1137/S1052623499362822

[17] Setoodeh, S., Blom, A. W., Abdalla, M. M., and Gürdal, Z., "Generating Curvilinear Fiber Paths from Lamination Parameters Distribution," *C47th AIAA/ASME/ASCE Structures, Structural Dynamics & Materials Conference*, Vol. 5, AIAA, Reston, VA, May 2006, pp. 3440–3452.

[18] Fukunaga, H., and Sekine, H., "Stiffness Design Method of Symmetric Laminates Using Lamination Parameters," *AIAA Journal*, Vol. 30, No. 11, 1992, pp. 2791–2793. doi:10.2514/3.11304

[19] Grenestedt, J. L., and Gudmundson, P., "Lay-Up Optimisation of Composite Material Structures," *Proceedings of IUTAM Symposium on Optimal Design with Advanced Materials*, Elsevier Science, Amsterdam, 1992, pp. 311–336.

[20] Setoodeh, S., Abdalla, M. M., and Gürdal, Z., "Approximate Feasible Regions for Lamination Parameters," *11th AIAA/ISSMO Multidisciplinary Analysis and Optimization Conference*, Vol. 2, AIAA, Reston, VA, May 2006, pp. 814–822.

[21] Bloomfield, M., Diaconu, C., and Weaver, P., "On Feasible Regions of Lamination Parameters for Lay-Up Optimization of Laminated Composites," *Proceedings of the Royal Society of London, Series A: Mathematical, Physical, and Engineering Sciences*, Vol. 465, No. 2104, 2009, pp. 1123–1143. doi:10.1098/rspa.2008.0380

[22] Rogers, D. F., *An Introduction to NURBS: With Historical Perspective*, Morgan Kaufmann, San Mateo, CA, 2000, pp. 179–185.

[23] Hughes, T., Cottrell, J., and Bazilevs, Y., "Isogeometric Analysis: CAD, Finite Elements, NURBS, Exact Geometry and Mesh Refinement," *Computer Methods in Applied Mechanics and Engineering*, Vol. 194, Nos. 39–41, 2005, pp. 4135–4195. doi:10.1016/j.cma.2004.10.008

[24] Cottrell, J. A., Hughes, T. J. R., and Bazilevs, Y., *Isogeometric Analysis: Toward Integration of CAD and FEA*, Wiley–Blackwell, New York, 2009, pp. 19–68.

[25] Nagy, A. P., Abdalla, M. M., and Gürdal, Z., "Design of Anisotropic Composite Shells Using an Isogeometric Approach," *13th AIAA/ISSMO Multidisciplinary Analysis and Optimization Conference*, AIAA Paper 2010-9181, 2010.

[26] Svanberg, K., "MMA and GCMMA, Versions September 2007," *Optimization and Systems Theory*, KTH, Stockholm, Sweden.

[27] Schmit, L., Jr., and Farshi, B., "Some Approximation Concepts for Structural Synthesis," *AIAA Journal*, Vol. 12, No. 5, 1974, pp. 692–699. doi:10.2514/3.49321

[28] Schmit, L., Jr., and Miura, H., "Approximation Concepts for Efficient Structural Synthesis," NASA Rept. CR-2552, pp. 1–14.

[29] Barthelemy, J.-F., and Haftka, R., "Approximation Concepts for Optimum Structural Design—A Review," *Structural Optimization*, Vol. 5, No. 3, 1993, pp. 129–144. doi:10.1007/BF01743349

[30] Starnes, J. H., Jr., and Haftka, R. T., "Preliminary Design of Composite Wings for Buckling, Strength and Displacement Constraints," *Journal of Aircraft*, Vol. 16, No. 8, 1979, pp. 564–570. doi:10.2514/3.58565

[31] Storaasli, O. O., and Sobieszczanski, J., "On the Accuracy of the Taylor Approximation for Structure Resizing," *AIAA Journal*, Vol. 12, No. 2, 1974, pp. 231–233. doi:10.2514/3.49201

[32] Fleury, C., and Braibant, V., "Structural Optimization: A New Dual Method Using Mixed Variables," *International Journal for Numerical Methods in Engineering*, Vol. 23, No. 3, 1986, pp. 409–428. doi:10.1002/(ISSN)1097-0207

[33] Svanberg, K., "Method of Moving Asymptotes—A New Method for Structural Optimization," *International Journal for Numerical Methods in Engineering*, Vol. 24, No. 2, 1987, pp. 359–373. doi:10.1002/(ISSN)1097-0207

[34] Yamazaki, K., "Two-Level Optimization Technique of Composite Laminate Panels by Genetic Algorithms," *37th AIAA/ASME/ASCE Structures, Structural Dynamics & Materials Conference*, Vol. 3, AIAA, Reston, VA, May 1996, pp. 1882–1887.

[35] Diaconu, C. G., and Weaver, P. M., "Approximate Solution and Optimum Design of Compression-Loaded, Postbuckled Laminated Composite Plates," *AIAA Journal*, Vol. 43, No. 4, 2005, pp. 906–914. doi:10.2514/1.10827

[36] Herencia, J. E., Weaver, P. M., and Friswell, M. I., "Optimization of Long Anisotropic Laminated Fiber Composite Panels with *T*-Shaped Stiffeners," *AIAA Journal*, Vol. 45, No. 10, 2007, pp. 2497–2509. doi:10.2514/1.26321

[37] Bloomfield, M. W., Herencia, J. E., and Weaver, P. M., "Analysis and Benchmarking of Meta-Heuristic Techniques for Lay-Up Optimization," *Computers and Structures*, Vol. 88, No. 5, 2010, pp. 272–282. doi:10.1016/j.compstruc.2009.10.007

[38] Wu, Z., Raju, G., and Weaver, P. M., "Buckling Analysis of VAT Plate Using Energy Method," *53th AIAA/ASME/ASCE Structures, Structural Dynamics & Materials Conference*, AIAA, Reston, VA, April 2012, pp. 1–12.

[39] Washizu, K., *Variational Methods in Elasticity and Plasticity*, 2nd ed., Pergamon, New York, 1975, pp. 159–206.

[40] Martin, A. F., and Leissa, A. W., "Application of the Ritz Method to Plane Elasticity Problems for Composite Sheets with Variable Fibre Spacing," *International Journal for Numerical Methods in Engineering*, Vol. 28, No. 8, 1989, pp. 1813–1825. doi:10.1002/(ISSN)1097-0207

[41] Raju, G., Wu, Z., Kim, B. C., and Weaver, P. M., "Prebuckling and Buckling Analysis of Variable Angle Tow Plates with General Boundary Conditions," *Composite Structures*, Vol. 94, No. 9, 2012, pp. 2961–2970. doi:10.1016/j.compstruct.2012.04.002

[42] Haftka, R. T., and Gürdal, Z., *Elements of Structural Optimization (Solid Mechanics and Its Applications)*, Springer, New York, 1991.

[43] Herencia, J. E., Haftka, R. T., Weaver, P. M., and Friswell, M. I., "Lay-Up Optimization of Composite Stiffened Panels Using Linear Approximations in Lamination Space," *AIAA Journal*, Vol. 46, No. 9, 2008, pp. 2387–2391. doi:10.2514/1.36189

[44] Van Campen, J. M. J. F., and Gürdal, Z., "Approximate Feasible Regions for Lamination Parameters," *50th AIAA/ASME/ASCE/AHS/ASC Structures, Structural Dynamics and Materials Conference*, AIAA, Reston, VA, April 2009.

[45] Pandey, M., and Sherbourne, A., "Postbuckling Behaviour of Optimized Rectangular Composite Laminates," *Composite Structures*, Vol. 23, No. 1, 1993, pp. 27–38. doi:10.1016/0263-8223(93)90071-W

[46] Gürdal, Z., and Olmedo, R., "In-Plane Response of Laminates with Spatially Varying Fiber Orientations: Variable Stiffness Concept," *AIAA Journal*, Vol. 31, No. 4, 1993, pp. 751–758. doi:10.2514/3.11613